Annales Societatis Geologorum Poloniae (2011), vol. 81: 133–160.

STUDIES ON MAGNETITE AND PYRITE MINERALIZATION, AND ON THEIR EARLY PALAEOZOIC OCEAN-FLOOR HOST-ROCKS FROM THE LESZCZYNIEC UNIT (WEST SUDETES, POLAND)

Teresa OBERC-DZIEDZIC[1], Ksenia MOCHNACKA[2], Wojciech MAYER[3], Adam PIECZKA[4], Robert A. CREASER[5] & Michał GÓRALSKI[6]

[1] *Institute of Geological Sciences, University of Wrocław, Plac M. Borna 9, 50-204 Wrocław, Poland, e-mail: teresa.oberc-dziedzic@ing.uni.wroc.pl*
[2] *AGH University of Science and Technology, Faculty of Geology, Geophysics and Environmental Protection, Department of Economic & Mining Geology, Al. Mickiewicza 30, 30-059 Kraków, Poland*
[3] *AGH University of Science and Technology, Faculty of Geology, Geophysics and Environmental Protection, Department of General Geology, Environment Protection and Geotourism, Al. Mickiewicza 30, 30-059 Kraków, Poland*
[4] *AGH University of Science and Technology, Faculty of Geology, Geophysics and Environmental Protection, Department of Mineralogy, Petrography and Geochemistry, Al. Mickiewicza 30, 30-059 Kraków, Poland*
[5] *Department of Earth & Atmospheric Sciences, University of Alberta, 1-26 Earth Sciences Building Edmonton, Alberta, Canada T6G 2E3*
[6] *AGH University of Science and Technology, Faculty of Management, Al. Mickiewicza 30, 30-059 Kraków, Poland*

Oberc-Dziedzic, T., Mochnacka, K., Mayer, W., Pieczka, A., Creaser, R.A. & Góralski, M., 2011. Studies on magnetite and pyrite mineralization, and on their early Palaeozoic ocean-floor host-rocks from the Leszczyniec Unit (West Sudetes, Poland). *Annales Societatis Geologorum Poloniae*, 81:133–160.

Abstract: The Leszczyniec Unit extends along the eastern margin of the Karkonosze-Izera Massif. It comprises the Early Palaeozoic, MORB-like Leszczyniec complex composed of metabasites, metagranites and metasediments. The metabasites host magnetite mineralization encountered in Jarkowice, whereas near Wieściszowice village the pyrite deposit occurs in metasediments and metabasites. The common feature of both sites is the almost complete absence of the accompanying ore minerals. Basing on petrographic, mineralogical, geochemical and microstructural studies, it was found that the metabasic rocks, which host magnetite mineralization, were lava flows, whereas the protoliths of pyrite-bearing schists were basic and acid tuffites accompanied by ocean-floor basalts. The igneous rocks from the Leszczyniec Unit were subjected to the ocean-floor metamorphism, whereas the accompanying sediments were altered by hydrothermal fluids enriched in sulphur ions, which reacted with iron derived from the sediment and promoted crystallization of pyrite. The sources of hydrothermal fluids were adjacent magmatic centres. The estimated age ~480 Ma for pyrite (Re-Os method) is similar to the previously known ~500 Ma age of metabasites (U-Pb, zircon method) from the Leszczyniec Unit, which establishes a temporal link between pyrite accumulation and the ocean-floor environment.

The rocks of the Leszczyniec Unit, first altered by the ocean-floor metamorphism and the hydrothermal fluids, were subsequently subjected to the regional metamorphism at 360–340 Ma and the two-stage deformations of various intensities, followed by the third stage of deformations which caused the reorientation of the regional foliation. The zones of ductile and brittle deformations connected with the second deformation event host the accumulations of magnetite formed at the expense of Fe-bearing rock-forming minerals or from iron supplied from adjacent sources. In the pyrite-bearing schists, mineral assemblages formed during the hydrothermal alteration have been subjected to recrystallization and were included into domains defining foliation and lineation, which formed during the first stage of deformation. Pyrite crystals were affected by both deformation stages. At the end of the second stage, the invasion of fluids led to the dissolution of pyrite crystals and to the filling of cracks in pyrite crystals with chalcopyrite and tennantite. This process was followed by the formation of quartz veins with minor amounts of ore minerals.

Key words: magnetite and pyrite mineralization, metabasites, ocean-floor metamorphism, paragonite, Leszczyniec Unit, Sudetes, Poland.

Manuscript received 25 November 2010, accepted 18 October 2011

INTRODUCTION

The meta-igneous Leszczyniec complex (Kryza & Mazur, 1995) bordering the eastern margin of the Karkonosze-Izera Massif (KIM) and composed of metabasites and metagranites has been interpreted to have formed in Early Palaeozoic time, in a MORB-like geologic setting. The meta-igneous rocks accompanied by metasediments are remnants of the obducted Saxothuringian basin floor (Mazur & Aleksandrowski, 2001). These rocks built the Leszczyniec Unit, which is the uppermost structural element of the Karkonosze-Izera Massif.

The Leszczyniec Unit hosts magnetite mineralization in Jarkowice and an abandoned uneconomic pyrite deposit in Wieściszowice. The occurrence of magnetite has not been previously described except for some recognition of disseminated, accessory magnetite in amphibolites (Szałamacha & Szałamacha, 1994). The small-scale mining activity in Jarkowice is documented by still identifiable, although inaccessible adits, small shafts and small waste dumps. Lis and Sylwestrzak (1986) reported after Schneider (1894) on mineable limonite accumulations in Jarkowice (German: Hermsdorf), at 912 m hill, but, in our opinion, correspondence between that site and our site is highly controversial. On the contrary, the pyrite deposit in Wieściszowice has been described in several publications (Berg, 1913; Petrascheck, 1933; Krajewski, 1949; Schneiderhöhn, 1955; Nielubowicz, 1958; Jaskólski, 1964). Recently, the area of the abandoned pyrite mine is protected as a landscape park.

This paper deals with the origin of magnetite and pyrite mineralization in the Leszczyniec Unit. The common feature of both mineralization sites is almost complete absence of other ore minerals accompanying magnetite or pyrite. Based on detailed petrographic, mineralogical, geochemical and microstructural observations, we evaluate the role of various genetic factors as well as reconstruct the mineralization process itself, the mineral succession, and the age of the formation of both occurrences. In a more general sense, our studies contribute to the knowledge of transformations within the fossil ocean floor.

GEOLOGICAL SETTING

The Karkonosze-Izera Massif (KIM) (Fig. 1) includes: (i) the Karkonosze granite pluton dated with different methods at 328–304 Ma (Pin *et al.*, 1987; Duthou *et al.*, 1991; Kröner *et al.* 1994; Machowiak & Armstrong, 2007), and (ii) some metamorphic complexes of various ages.

Mazur and Aleksandrowski (2001) have interpreted the metamorphic part of the KIM as a succession of four structural units – nappes (Fig. 1): (l) the Izera-Kowary Unit, (2) the Ješted Unit, (3) the Southern Karkonosze Unit, and (4) the Leszczyniec Unit. The uppermost position in this stack of nappes is occupied by the Leszczyniec Unit.

The Leszczyniec Unit includes the Early Ordovician (505±5 and 494±2 Ma, U-Pb zircon method; Oliver *et al.*, 1993) meta-igneous Leszczyniec complex (Kryza & Mazur, 1995) composed of fine-grained, schistose and medium-grained, massive metabasites as well as metagranites (felsic gneisses) and metadiorites (hornblende gneisses), the latter two forming several, large igneous bodies within the metabasites. The meta-igneous rocks of the Leszczyniec complex show geochemical signature typical of the N-MORB (Kryza *et al.*, 1995; Winchester *et al.*, 1995), except for metadiorites, which can be genetically related to the island arc lavas (Narębski, 1980), or can be the products of contamination of rift magmas with the crustal rocks (Kryza *et al.*, 1995). The Leszczyniec complex might have originated in an extensional rift environment (Kryza *et al.* 1995) although large amounts of felsic rocks preclude a mature, mid-ocean rift (Mazur & Aleksandrowski, 2001). In the northern part of the Leszczyniec Unit, near Wieściszowice village, the meta-igneous rocks are accompanied by pyrite-bearing schists. These schists represent the only metasedimentary rocks in that unit.

The Leszczyniec Unit rocks were deformed in the course of three deformation events (Mazur, 1995). The first deformation event D_1 produced penetrative foliation S_1, which strikes N–S to NNE–SSW and dips mostly to the ESE or WNW, and penetrative stretching lineation L_1 which plunges to the NNE or NE at a low or moderate angle. According to Mazur and Aleksandrowski (2001), the stretching lineation L_1 was produced by penetrative, sinistral shear, "*associated with a subduction-related underthrusting of the Leszczyniec Unit beneath the upper plate margin*" (Mazur & Aleksandrowski, 2001, p. 356). The first deformation event D_1 corresponded to the period of nappe emplacement. Based on ^{40}Ar-^{39}Ar white mica age from the HP rocks of the South Karkonosze nappe (Maluski & Patočka, 1997), the period of nappe stacking took place between 360 and 340 Ma (Mazur & Aleksandrowski, 2001). In the Leszczyniec Unit, the first deformation event D_1 was accompanied by metamorphism corresponding to greenschist-to-epidote-amphibolite-facies conditions (Kryza & Mazur, 1995).

The D_2 deformation event was connected with top-to-SE extensional collapse, which took place at ~340 Ma, before the Karkonosze granite emplacement (Mazur & Aleksandrowski, 2001). In the Leszczyniec Unit, it produced new, penetrative foliation S_2 along the contact zone with the Izera-Kowary Unit and localized brittle-ductile deformation zones within the unit (Mazur & Aleksandrowski, 2001). The L_2 lineation trends WNW–ESE. The axes of F_1 and F_2 folds formed during the D_1 and D_2 deformation events are generally parallel to the L_1 and L_2 lineations, respectively.

During the D_3 deformation event, the regional foliation became steeper, locally nearly vertical. This reorientation is attributed to a rotation around a NNE–SSW-trending axis of the so-called East Karkonosze Monocline (Oberc, 1960; Mazur & Aleksandrowski, 2001). The rotation post-dated the emplacement of the Karkonosze granite and affected not only the metamorphic complexes at the eastern margin of the KIM, but also the Upper Visean conglomerates of the Szczawno Formation in the adjacent Intra-Sudetic Basin (Dziedzic & Teisseyre, 1990). The Biały Kamień beds of the Westphalian age, which unconformably overlie the Szczawno Formation (Dziedzic & Teisseyre, 1990) provide the upper time limit for the origin of the East Karkonosze monocline (Mazur & Aleksandrowski, 2001).

The rocks of the Leszczyniec Unit host several occurrences of ore minerals. The largest is the well-known, un-

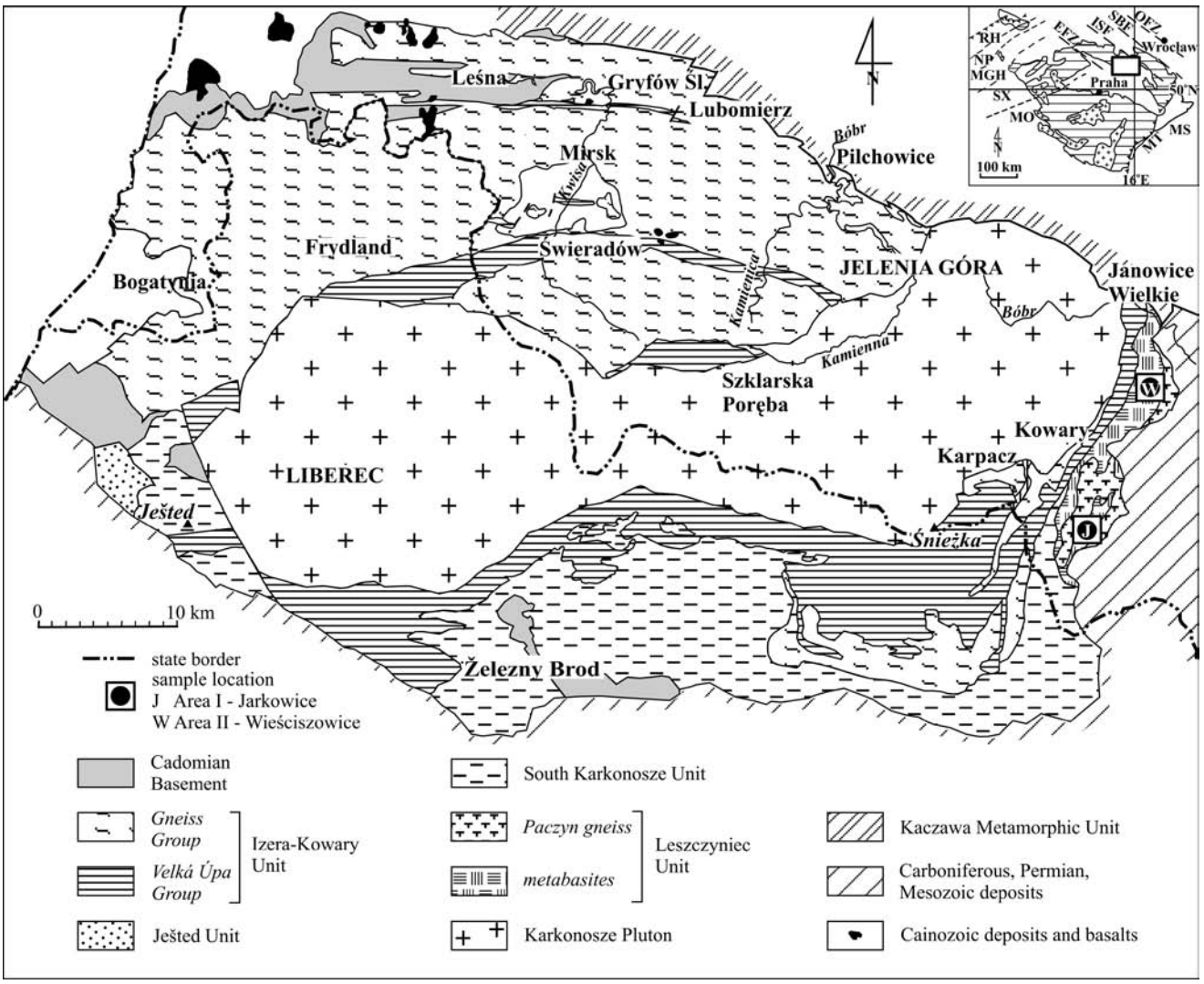

Fig. 1. Geological sketch map of the Karkonosze-Izera Massif (compiled from Chaloupský *et al*., 1989; Mazur, 1995; Mazur & Aleksandrowski, 2001; Oberc-Dziedzic, 2003; Oberc-Dziedzic *et al*., 2010). KIM – Karkonosze-Izera Massif. Inset map: EFZ – Elbe Fault Zone, ISF – Intra-Sudetic Fault, MGH – Mid-German High, MO – Moldanubian Zone, MS – Moravo-Silesian Zone, NP – Northern Phyllite Zone, OFZ – Odra Fault Zone, RH – Rhenohercynian Zone, SBF – Sudetic Boundary Fault, SX – Saxothuringian Zone, TB – Teplá-Barrandien Zone. Rectangle shows the position of the KIM in the Bohemian Massif

economic pyrite deposit at Wieściszowice. The newly discovered sites are: the Jarkowice magnetite occurrence and the traces of sulphide mineralization in Ogorzelec. Moreover, some vein-type occurrences and deposits, *e.g.*, at Miedzianka, hosted in adjacent structural units extend to the northern part of the Leszczyniec Unit. Below, the magnetite mineralization at Jarkowice (Area I) and the pyrite deposit at Wieściszowice (Area II) are described and discussed.

MATERIALS AND METHODS

The laboratory analyses aimed to: (1) recognize petrographic features and geochemical signature of the host-rocks, and chemical composition of rock-forming and ore minerals; (2) establish the mineral succession and parageneses, and determine the conditions of metamorphism; (3) determine the formation age of pyrite.

The petrographic observations were performed on polished surfaces and oriented sections of hand specimens as well as on 28 thin sections examined under the polarizing microscope.

The chemical composition of rock-forming minerals was analysed at the Joint-Institute Analytical Complex for Minerals and Synthetic Substances, Faculty of Geology, University of Warsaw. Analyses were carried on 6 specimens using the CAMECA SX 100 electron microprobe (EMP) at the acceleration voltage 15 kV, the electron beam current 10 nA for analyses of plagioclases and micas, and 20 nA for other minerals, a counting time 20 s and a background time of 10 s. The standards included both the minerals and the synthetic substances. The raw data were processes with the ZAF procedure contained in the PAP software supplied by the CAMECA.

The observations of ore minerals were made under the ore microscope on 33 polished sections. The microprobe

chemical analyses of selected ore minerals were carried out at the above mentioned laboratory of the University of Warsaw.

The chemical analyses were run for 9 whole-rock samples at the ACTLABS laboratory in Canada with the combined ICP- OES and ICP-MS methods (the ACTLABS code "4Lithores") including determination of major and trace elements.

The isotopic age of pyrite from the Wieściszowice deposit was determined with the Re-Os method at the University of Alberta, Canada. Four samples were selected, from which a few milligrams of pyrite was separated and the Re content were determined by isotope dilution method. Seven Re-Os analyses were then completed, following the methods for "Low-Level Highly Radiogenic" sulfide minerals outlined by Morelli *et al.* (2004, 2005).

The geothermometric analyses of fluid inclusions were carried out at the Department of Mineral Deposits and Mining Geology, Faculty of Geology, Geophysics and Environmental Protection, AGH University of Science and Technology in Kraków. Selected samples of quartz veins exposed at the Wieściszowice deposit were used. From samples doubly polished, 200 μm-thick sections were examined with the Linkam THMS 600 heating–freezing stage equipped with the TMS 93 module and the Linkam LNP pump, all attached to the Nikon Eclipse E6000 microscope. Observations were made with the Ikegami video camera and the Linkam VTO 232 video panel. The measurement system was calibrated with the special thin section that contained inclusions of pure CO_2. During observations the FI sections were abruptly frozen down to –120°C (occasionally down to –198°C) in order to avoid the formation of metastable phases. This procedure enabled us to reveal the presence of gases other than carbon dioxide. The heating rates were: 5–10°C/min to the room temperature (reduced to 0.5°C close to phase transformation points), then 20°C/min to 100°C and 5–10°C/min for higher temperatures. For low temperatures, the accuracy of measurement was 0.1–0.2°C.

The samples were thoroughly selected and subjected to comprehensive examinations with most of the methods mentioned above. A few samples were analysed with all these methods.

The mineral abbreviations used in this study originate from Kretz (1983) and from Whitney and Evans (2010).

Documentation of the research (samples, thin and polished sections, results of whole-rock, EMP and other analyses, and photo documentation) are in the possession of two of us (K. Mochnacka and T. Oberc-Dziedzic).

ORE MINERALIZATION IN THE META-IGNEOUS LESZCZYNIEC COMPLEX – AREA I - JARKOWICE

The Area I includes the exposures of amphibolites with magnetite mineralization located in the southern part of the Leszczyniec Unit, NE from Jarkowice village (Fig. 1). Mineralization is hosted in a series of metabasites identified as actinolitic amphibolites (Szałamacha, 1969).

The ore mineralization from this area has not been previously described in detail. However, numerous old workings: two adits, a few small shafts following the general, NE–SW trend, and a small waste dump, all document the past activity of unknown age. Moreover, during the field work magnetite has been found in exposures and in rubble, close to the old mine workings. In some exposures zones with macroscopically visible pyrite were encountered, as well.

Petrography of rocks from the Area I - Jarkowice

Streaky amphibolite (J1) is a green, fine-grained rock. The foliation is defined by layers composed of elongated albite blasts and streaks of parallel hornblende blasts, among which aggregates of magnetite and epidote grains are scattered (Fig. 2A). Epidote forms also lenses together with bluish-green hornblende and, sometimes, also with albite. Moreover, the rock contains euhedral porphyroblasts of epidote and ellipsoidal, 2.5 mm long nodules composed of radial aggregates of actinolite surrounded by epidote grains (Fig. 2B). Both the epidote porphyroblasts and the nodules show signs of rotation and have strain shadows filled with bluish-green hornblende (Fig. 2B).

The protolith of streaky amphibolite is difficult to identify. Distinct foliation may suggest a primarily bedded rock. However, it seems likely that well-developed lamination resulted rather from deformation of an igneous rock, presumably coarser-crystalline than the protolith of vesicular amphibolite J2.

Amphibolite with segregation vesicles (J2) is a dark-green rock with obscured streaky structure and macroscopically observable nodules, 2–4 mm long, of indistinct boundaries. The foliation is defined by up to 0.2 mm long, parallel blasts of hornblende with bluish-green pleochroism, as well as elongated blasts of albite, about 0.1 mm long. Also parallel to the foliation are streaks composed of somewhat larger blasts of hornblende and epidote. In some specimens aggregates of minute magnetite grains are arranged parallel to the foliation.

The ellipsoidal nodules reveal concentric structures with actinolite in the marginal zones and epidote, albite and hornblende forming the cores. These nodules are presumably the segregational vesicles observed in the ocean-floor basalts. Such vesicles are partly or entirely filled with the melt segregated out from the surrounding magma (Smith, 1967), which discerns such forms from amygdaloids filled with hydrothermal minerals left after crystallization of magma (Vernon, 2004). Although mineral composition of nodules has changed during the metamorphism, their concentric structure seems to reflect the successive crystallization of basaltic magma. Certainly, the nodules are pre-metamorphic structures, as revealed by signs of rotation, haloes and strain shadows composed of minerals identical with those, which define foliations of the rocks.

Massive amphibolite (J3) is a dark-green, aphanitic rock of random texture. The matrix (Fig. 2C) consists of cloudy albite-epidote aggregates, which host randomly arranged, acicular actinolite, pale-green hornblende, up to 0.2 mm long, magnetite grains, and very rare, 2-mm-long pseudomorphs after pyroxene filled with radial actinolite aggregates and surrounded by epidote rims.

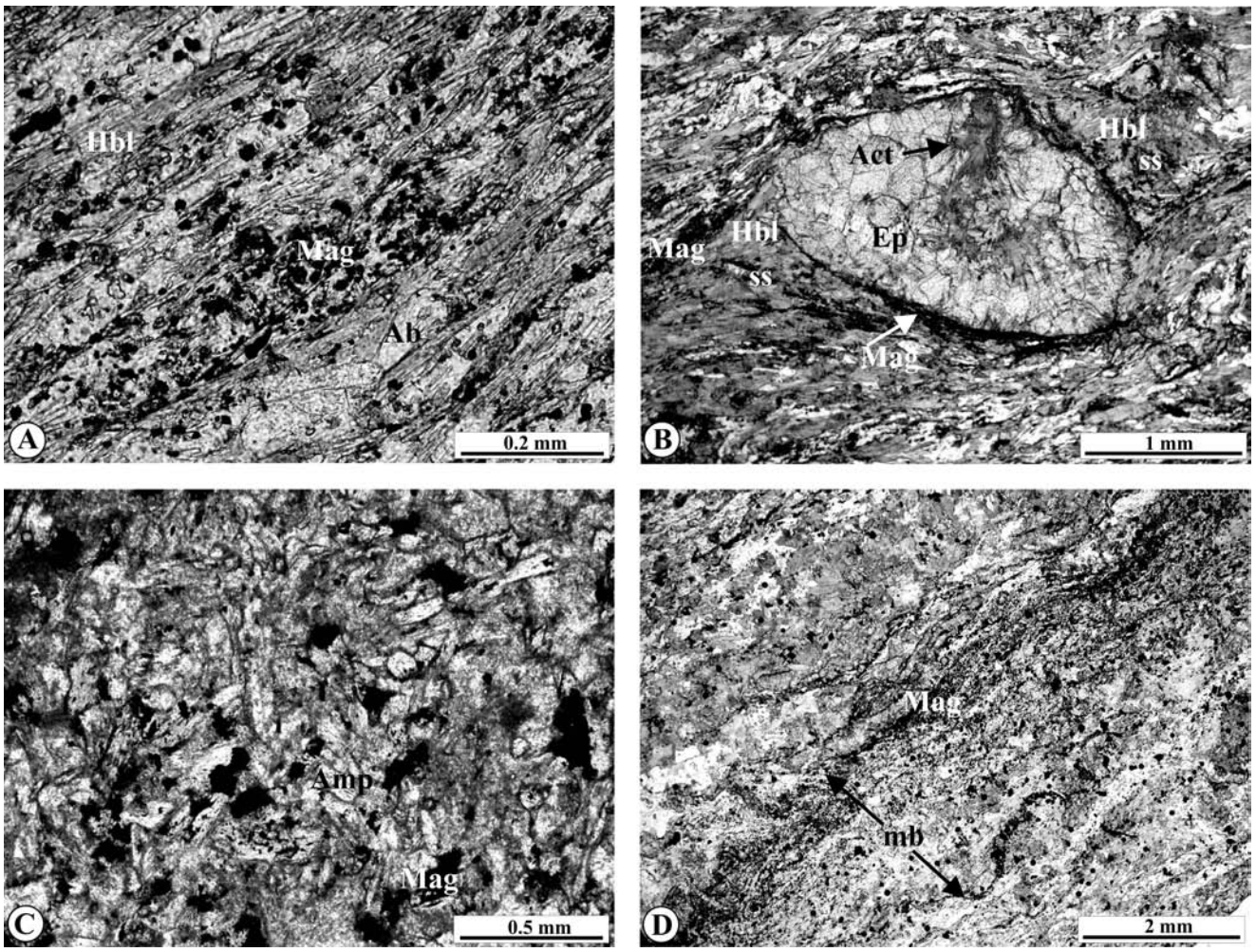

Fig. 2. **A** – magnetite aggregates parallel to foliation defined by laths of amphibole and plagioclase in *streaky amphibolite*; **B** – ellipsoidal nodule composed of epidote crystals in *streaky amphibolite*; in the central part of nodule radial actinolite aggregates occur; cone-shape strain shadows (ss) adjacent to nodule are filled with bluish-green hornblende; **C** – mineral framework of *massive amphibolite*: cloudy albite-epidote aggregate with randomly arranged amphibole laths and magnetite crystals; **D** – thin, cord-like magnetite aggregates embedded in mylonite zone (mb) parallel to the foliation A-D, plane-polarized light. Hbl – hornblende, Mag – magnetite, Ab – albite, Act – actinolite, Amp – amphibole, Ep – epidote

The amphibolites from Jarkowice presumably represent various parts of a primary, ocean-floor lava flow.

Metamorphism of amphibolites in the Area I - Jarkowice

The metamorphic events were recorded by parageneses:

I. bluish-green hornblende + albite + epidote + magnetite, which defines the foliation. The hornblende is also present in the strain shadows around the nodules;

II. pale green hornblende + actinolite + albite + epidote + magnetite, which is characteristic for the massive amphibolite.

Actinolite is also present in the streaky amphibolite, in strain shadows around rotated epidote porphyroblasts and nodules. The rotation of porphyroblasts and nodules was probably coeval with the reactivation of the foliation defined by bluish-green hornblende and proceeded during the decreasing temperature, as documented by the presence of actinolite in some strain shadows. Further decrease of temperature is proved by chlorite, which crystallized along extension fractures parallel to the axial surfaces of the youngest folds.

Although actinolite and chlorite are present in places, amphibolites do not show signs of general retrogression, such as actinolite rims around the hornblende grains or chloritization of amphiboles. The retrogresion is confined to the zones of intensive deformation.

Ore mineralization in the Area I - Jarkowice

Magnetite mineralization in the Area I - Jarkowice

In all amphibolite varieties from the Area I - Jarkowice, magnetite forms disseminated grains or aggregates. Magnetite layers and lenses, magnetite-quartz aggregates, as well as magnetite in breccias are confined to deformation zones.

Disseminated magnetite

Disseminated magnetite occurs in massive amphibolite (J3, Fig. 2C) where it forms randomly arranged grains, and

in foliated amphibolites (J1, J2) where it forms concentrations following the foliation or surrounding the nodules (Fig. 2A, 2B).

Magnetite layers and lenses

Amphibolites from Jarkowice reveal poorly visible or macroscopically invisible zones of intensive, mylonitic deformation, from 3 mm to 2 cm thick, concordant with the foliation. The mylonitization is documented by the reduction of grain size. The zones are composed mostly of chlorite and are enriched in quartz, epidote and magnetite in comparison to the enclosing rock.

The simplest forms of magnetite accumulations hosted within the mylonitic zones are thin, *cord-like aggregates* (Fig. 2D).

The thicker (1–3 cm) *magnetite layers and lenses* composed of several types of domains (Fig. 3A, 3B) often follow the zones of pre-existing crenulation cleavage (Fig. 3C), which seem to be particularly susceptible to mylonitization. In mylonitization zones the oldest mineral was chlorite I, showing violet interference colours, followed by disseminated epidote. Chlorite I, arranged in crenulations, was partly replaced by magnetite. The habit of magnetite grains suggests their formation as pseudomorphs after chlorite or amphibole (Fig. 3C). Further development of mylonitization zones was accompanied by recrystallization connected with differentiation into domains 1–5 and with the crystallization of larger, euhedral or rounded magnetite grains, the latter subjected to disruption into the V-pull-apart structures filled with chlorite I (Fig. 3D). During the following stage of recrystallization, the epidote domains were formed (Fig. 3E, F). In their neighbourhood, magnetite strain caps and strain shadows filled with chlorite II originated (Fig. 3B). These structures document the active deformation process. Further deformation resulted in cracking of epidote domains. The cracks in these domains were filled with chlorite II showing olive-brown interference colours. Bending of flakes of this chlorite variety indicates displacements along the cracks (Fig. 3G).

Magnetite-quartz aggregates

Such aggregates resemble streaky quartzite (variety A, Fig. 4A) or massive quartzite (variety B, Fig. 4C).

The variety A is composed of isometric quartz grains, 0.2 mm in diameter, among which magnetite "dust" is disseminated or accumulated in streaks and discontinuous laminae, up to 3 mm thick (Fig. 4B). Locally, recrystallized zones appear. They host euhedral magnetite grains, green, weakly pleochroic chlorite and scarce epidote. The rock is cut by fractures filled with quartz veinlets (Fig. 4A, B), locally accompanied by chlorite, with chlorite or, rarely, with calcite.

The variety B (Fig. 4C) is a massive breccia composed of three types of quartz domains cemented with magnetite aggregates (Fig. 4C, D). In the vicinity of magnetite aggregates quartz grains are larger, which indicates recrystallization, and chlorite blasts appear, as well.

Magnetite is accompanied by minor amounts of hematite (possibly martite). Hematite forms crystals accumulated around the margins of magnetite grains. Rarely, hematite also occurs as lamellae within the magnetite. In some samples magnetite aggregates are accompanied by pyrite.

Magnetite in amphibolite and epidote breccias

Such magnetite fills the network of fine cracks cutting the amphibolite cataclasites (Fig. 4E) or larger epidote aggregates (Fig. 4F).

Pyrite mineralization in the Area I - Jarkowice

Apart from pyrite accompanying magnetite, pyrite variety related to the zones of fractures in amphibolites occurs, as well. Pyrite forms spotty aggregates or single, large crystals replaced to various degree with Fe-hydroxides (Fig. 4G).

Chemical composition of magnetite and other ore minerals

The chemical analyses of magnetite did not indicate significant admixtures of trace elements, except for vanadium (0.08 wt.% V_2O_3, Table 1), cobalt (0.04 wt.% CoO) and titanium (0.06 wt.% TiO_2).

Table 1

Selected electron microprobe analyses (in wt %) and formulae of magnetite and titanite from the Area I - Jarkowice

	Titanite		Magnetite
SiO_2	29.64	29.61	0.00
Ta_2O_5	0.22	0.18	0.00
FeO	n.a.	n.a.	30.58
Fe_2O_3	1.47	1.52	67.97
MnO	0.02	0.02	0.02
TiO_2	37.22	35.81	0.06
CaO	28.22	27.77	0.00
Al_2O_3	1.08	1.69	0.00
V_2O_3	n.a.	n.a.	0.08
Cr_2O_3	n.a.	n.a.	0.11
NiO	n.a.	n.a.	0.03
CoO	n.a.	n.a.	0.04
Total	97.87	96.6	98.89
Number of ions (a.p.f.u.)			
Si	0.984	0.992	0.000
Ta	0.002	0.002	0.000
Fe^{2+}	n.a.	n.a.	0.996
Fe^{3+}	0.037	0.038	1.992
Mn	0.001	0.001	0.001
Ti	0.930	0.903	0.002
Ca	1.004	1.997	0.000
Al	0.042	0.067	0.000
V	n.a.	n.a.	0.002
Cr	n.a.	n.a.	0.003
Ni	n.a.	n.a.	0.001
Co	n.a.	n.a.	0.001

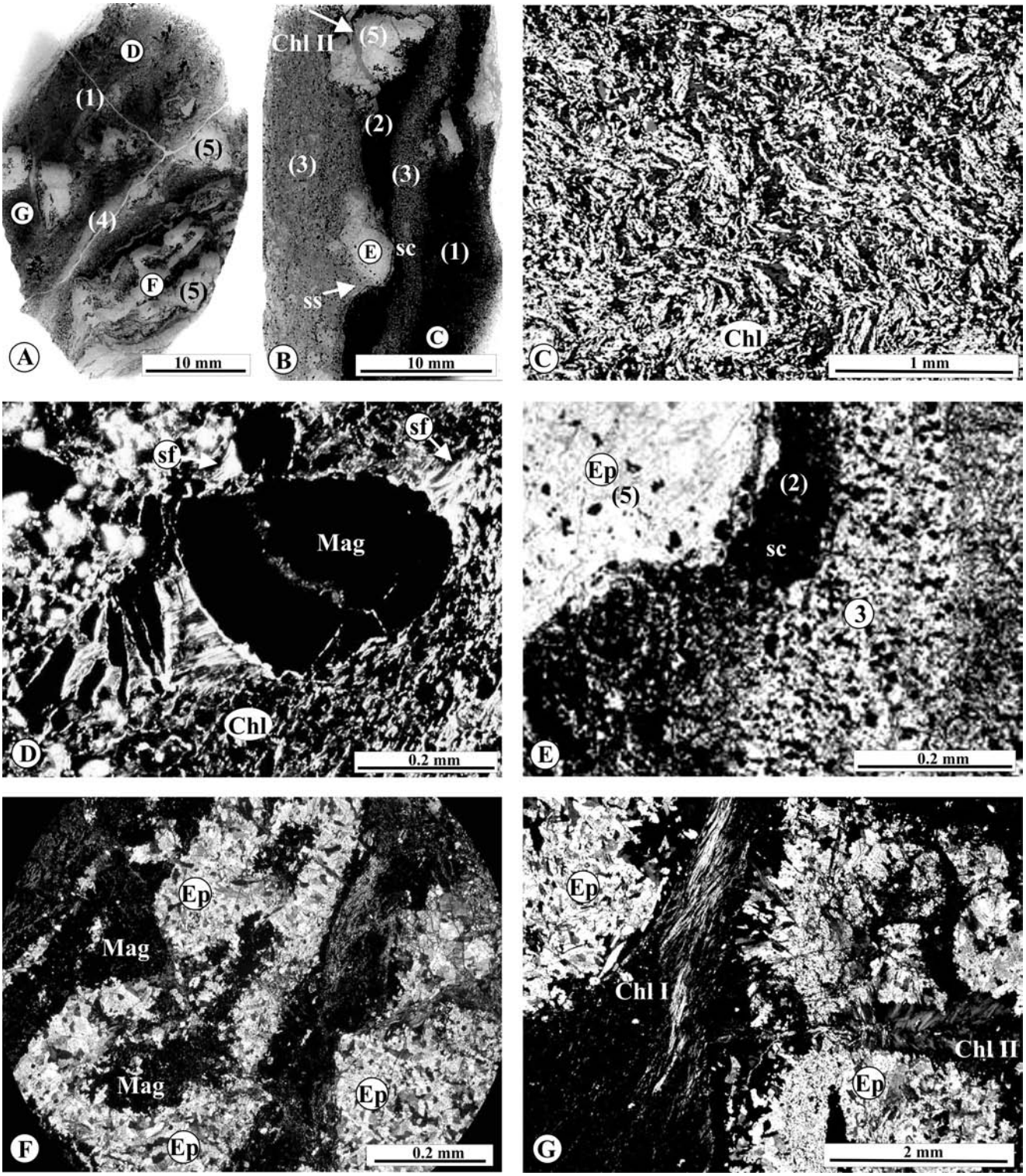

Fig. 3. **A, B** – microscopic images of magnetite laminae; domains: (1) chlorite I-magnetite, (2) magnetite-chlorite I, (3) epidote-chlorite II-magnetite, (4) chlorite II-epidote, (5) epidote; capital letters mark specific details in Fig. 3C-G; ss-strain shadow, sc-strain cap; **C** – domain (1); chlorite I (dark) and magnetite (white) arranged in folds resembling crenulations, reflected light; **D** – rounded crystal of magnetite in domain (1); V-pull-apart structure: fractures between magnetite grain and its split fragments are filled with chlorite I, which forms also strain fringes (sf) around magnetite grains, plane-polarized light; **E** – domain (2) between domains (3) and (5) associated with strain cap (sc) formed from domain (2), enriched in magnetite and devoid of chlorite I, plane-polarized light; **F** – domain (5) rimmed with magnetite and hosting magnetite aggregates inside, resembling the atoll structures, crossed polars; **G** – epidote domains (5) separated by shearing zones filled with fibrous chlorite I; chlorite II fills the crack in domain (on the right), crossed polars. Chl – chlorite, Ep – epidote, Mag – magnetite


Mag
A
10 mm

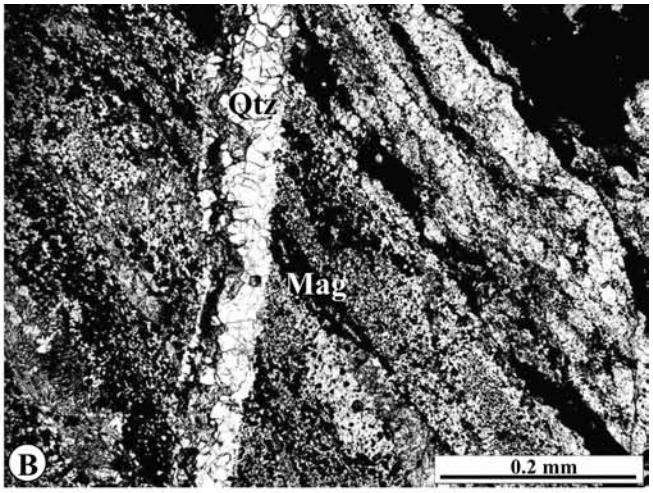
Qtz
Mag
B
0.2 mm

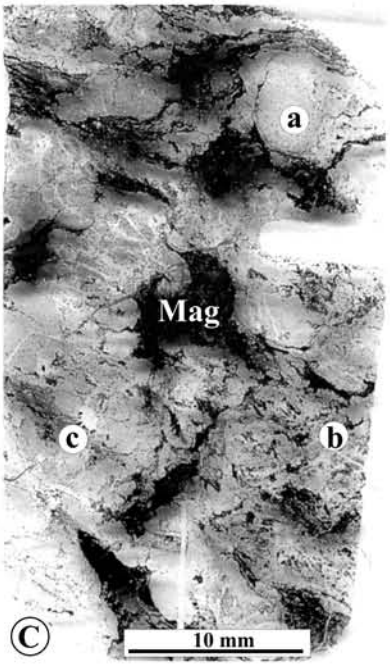
a
Mag
c
b
C
10 mm

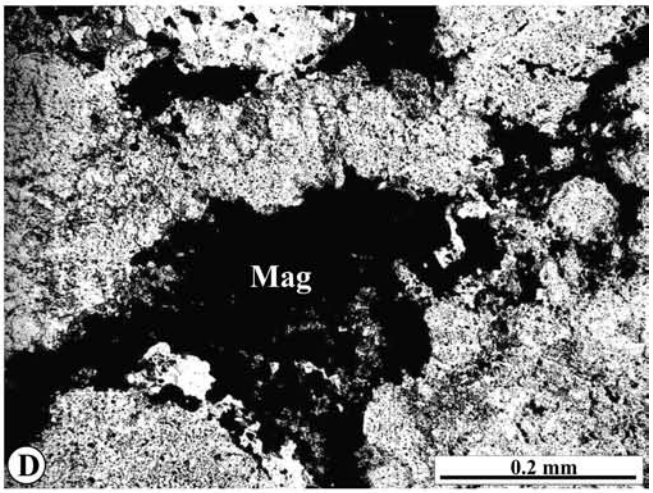
Mag
D
0.2 mm

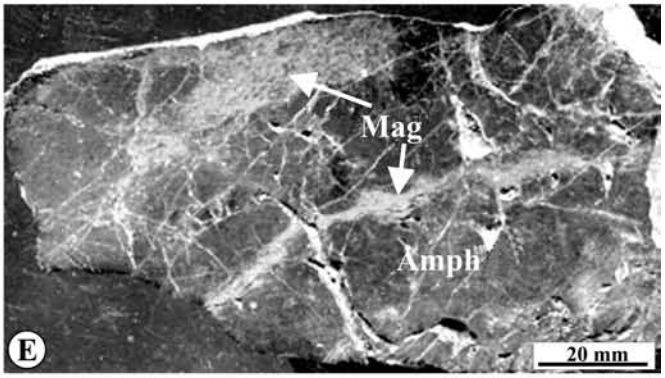
Mag
Amph
E
20 mm

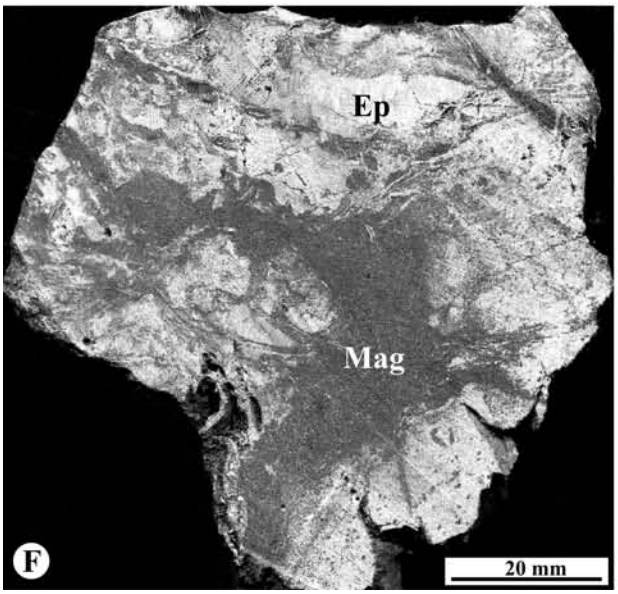
Ep
Mag
F
20 mm

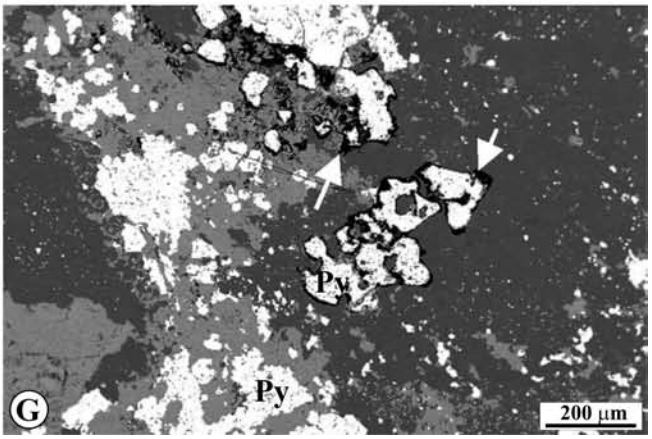
Py
Py
G
200 μm

Titanite crystals contain increased amounts of Al_2O_3 (1.08 wt.%) and Fe_2O_3 (up to 1.52 wt.%). Important are also admixtures of Ta_2O_5 (0.22 wt.%; Table 1).

Pyrite accompanying magnetite accumulations shows stoichiometric composition, except for some grains which revealed small amounts of Co (up to 0.26 wt.%; Table 2).

ORE MINERALIZATION IN THE META-IGNEOUS LESZCZYNIEC COMPLEX – THE AREA II - WIEŚCISZOWICE

The Area II is located in the northern part of the Leszczyniec Unit, in the vicinity of Wieściszowice village. In the eastern part of the Area II, a packet of pyrite-bearing schists occurs, about 100 m thick. The western part is built of mafic rocks (amphibolites). The rocks strike north- south and dip to the east at about 50°.

The pyrite deposit in Wieściszowice had been intermittently mined between the half of the 18th and the beginning of the 20th centuries, and again, in the years 1905–1925 (Fedak & Lindner, 1966). Monthly production was up to 600 tons of pyrite concentrate, grading 47 wt.% sulphur and 0.5 wt.% copper (Berg, 1938).

The of pyrite deposit was described by Nielubowicz (1958) and Jaskólski (1964) who based on data from drillings completed in the years 1953–1954 and on field observations in the open pit. Later descriptions of rocks from Wieściszowice, based on observations in the outcrops, were published by Teisseyre (1973) and by Szałamacha and Szałamacha (1991).

Mineralization in quartz veins was described by Piestrzyński and Salamon (1977).

According to Jaskólski (1964), the bottom series comprises quartz schists, brecciated and cemented with limonite at the boundary with the ore series. The top series includes chlorite schists. The ore series consists of many varieties of quartz-sericite-chlorite schists, which mineral composition depends on proportions between these three components (Jaskólski, 1964). The schists host randomly disseminated pyrite accompanied by traces of chalcopyrite and galena. During the mining operations, three zones of a high-grade pyrite ore of thickness from 5 to 12 m were encountered (Berg, 1913). The ore mineralization gradually ceases both upwards and downwards across the schist sequence (Jaskólski, 1964). The ore series is cut by quartz veins with poor sulphide mineralization.

According to Jaskólski (1964), the Wieściszowice pyrite deposit is of effusive-sedimentary exhalative origin, whereas the vein mineralization was formed due to metamorphic remobilization of elements; precisely, it resulted from "*the metamorphic hydrothermal activity*".

Table 2

Selected electron microprobe analyses (in wt %) and formulae of pyrite from the Area I - Jarkowice

	1	2	3
S	52.00	52.39	52.31
Sb	0.00	0.00	0.00
As	0.03	0.02	0.02
Fe	46.59	46.78	46.58
Cu	0.00	0.00	0.00
Ni	0.05	0.06	0.00
Co	0.26	0.03	0.02
Mn	0.00	0.00	0.00
Total	98.94	99.27	98.94
Number of ions (a.p.f.u.)			
S	1.932	1.947	1.955
Sb	0.000	0.000	0.000
As	0.000	0.000	0.000
Fe	0.994	0.998	1.000
Cu	0.000	0.000	0.000
Ni	0.001	0.001	0.000
Co	0.005	0.001	0.000
Mn	0.000	0.000	0.000

The pyrite ore body has an extensive weathering zone. Its mineralogy has been comprehensively studied by Parafiniuk (1991, 1996) and Parafiniuk *et al.* (2010).

Petrography of rocks from the Area II - Wieściszowice

In the Area II, studies were carried on amphibolites from an abandoned quarry located west from the Wieściszowice village and on pyrite-bearing schists exposed in the abandoned open pit located east of the amphibolite quarry. From the structural point of view, the pyrite-bearing schists cover the amphibolites. Below, the rocks have been described in the order from west to east.

Amphibolites

Streaky amphibolite (sample W6), exposed in the upper, western level of amphibolite quarry, is a very fine-grained rock of well-visible foliation underlain by thin, light-green streaks. The rock matrix comprises amphibole, titanite,

Fig. 4. **A** – microscopic image of magnetite accumulation resembling streaky quartzite (variety A), cracks filled with quartz; **B** – streaks and discontinuous laminae composed of magnetite "dust" between quartz grains; crack arranged at high angle to streaks is filled with 0.5-mm-thick quartz veinlet (variety A), plane-polarized light; **C** – microscopic image of magnetite accumulation resembling breccia (variety B), composed of rounded quartz domains devoid of magnetite "dust" (a); quartz domains with magnetite "dust" (b) and angular domains resembling variety A (c) cemented with magnetite aggregates having fringed edges; **D** – magnetite aggregates (variety B), plane-polarized light; **E** – network of magnetite veinlets in amphibolitic cataclasite (Amph); **F** – magnetite coexisting with epidote; **G** – nest-like and disseminated pyrite, traces of replacement with Fe-hydroxides are visible (white arrow), BSE image. Ep – epidote; Mag – magnetite, Py – pyrite, Qtz – quartz

epidote and ilmenite with rims of titanite. The composition of the inner parts of amphibole grains corresponds to actinolite or Mg-hornblende whereas the outer zones are enriched in Al, *i.e.*, these correspond to tschermakite. In the matrix, porphyroblasts of epidote and plagioclase arranged in folded streaks can be observed. The plagioclase porphyroblasts show high contents of anorthite (up to 41%) and spots of albite. Some plagioclase porphyroblasts are rotated and have albite and actinolite in the strain shadows. Actinolite crystallized also in cracks within the porphyroblasts. Epidote forms larger lenses or microscopic-size laminae, which results in a streaky structure of the rock. Apart from epidote, these laminae contain also $An_{32.5}$ plagioclase, diopside and larger blasts of dark-green amphibole of composition corresponding to magnesiohornblende and to tschermakite.

The streaky amphibolite reveals the lack of mineral equilibrium, as documented by the coexistence of Ca-rich plagioclases with albite and tschermakite with actinolite, and the presence of zonality. Such lack of mineral equilibrium together with the presence of pyroxene resulted from the interference of thermal aureole of the adjacent Karkonosze granite and the earlier, lower-temperature mineral parageneses formed during the regional metamorphism.

Calcitic amphibolite (sample W7), which crops out at the lower level of amphibolite quarry, is a dark-green rock with characteristic, light-green, shredded domains. Under the microscope, one can observe perfect foliation defined by streaks of dark-green hornblende, lighter laminae composed of plagioclase and epidote, and calcite laminae of various thicknesses. Calcite forms also the younger veinlets cutting the foliation. The older foliation has been preserved within lensoidal domains (microlithons). It is defined by the same mineral assemblage and arranged under high angle to the laminae. The calcitic amphibolite is rich in opaque minerals.

Pyrite-bearing schists

The minerals mentioned in the names of particular pyrite-bearing schists follow the order corresponding to their decreasing contents in the rocks. All schists display well-visible, penetrative foliation and stretching lineation.

Chlorite-muscovite-(paragonite)-albite schists (sample W2) are exposed in the western part of the open pit, in large, smooth walls inclined to the NE. These are light-grey rocks, yellowish when weathered, very rich in pyrite. The very fine-grained matrix includes white mica, chlorite, albite and titanite, and large crystals of pyrite surrounded by fibrous quartz or chlorite forming the strain fringes (Fig. 5A). The white micas are represented by Na-K mica (paragonite-muscovite) and, less commonly, by K-Na mica and muscovite. In the matrix, the intimate intergrowths of Na-K mica and chlorite are observed. Strongly elongated pyrite crystals are arranged parallel to the boundaries of mica-chlorite intergrowths (Fig. 5B). The paragonite-muscovite mica rarely forms also larger (0.1 mm), rotated plates, which are presumably the detrital grains (Fig. 5C). The shredded terminations of plates are enriched in potassium. The younger generation of white mica is muscovite, which forms plates intergrown with chlorite and arranged obliquely to the older plates of chlorite and paragonite-muscovite (Fig. 5D).

Chlorite-albite-quartz-muscovite schists (sample W3) are greyish-green rocks of indistinct, glittering foliation surfaces, very rich in pyrite. The rocks contain lenticular chlorite-muscovite domains rich in pyrite and quartz-albite-muscovite domains, in which pyrite crystals are less common and smaller. Chlorite and muscovite plates, and elongated albite and quartz crystals are arranged parallel to the boundaries of the domains. Other components seen in the matrix are titanite and scarce rutile. Albite from the matrix can be overgrown by muscovite (Fig. 5E). Pyrite forms euhedral crystals with perfect strain fringes composed of quartz in domains rich in quartz and albite (Fig. 5F), and with chlorite fringes in chlorite-rich domains.

Quartz-albite schists (sample W4) can be observed in the central part of the open pit. The cream-coloured rocks have macroscopically distinct lamination and contain large amounts of pyrite. Layers of grey quartz are up to 1 cm thick. Such layers contain rare plates of white, K-Na mica. The largest muscovite plate is rotated (Fig. 6A). Due to weathering and action of fluids, a part of white mica plates were transformed into hydromica. Moreover, the action of fluids resulted in the formation of dolomite. Its crystals are arranged parallel to the foliation or fill the cracks (Fig. 6A). Dolomite penetrated also the matrix, forming amoebic ”spots” between the quartz grains. In such spots minute grains of fluorite were found (Fig. 6B). Dolomite forms also rims around pyrite crystals (Fig. 6C), which are older than quartz strain fringes (Fig. 6C).

Muscovite-quartz-albite schists (sample W1) form an extended exposure in the central part of the open pit. Unweathered schists of this type are silver-grey with silky luster whereas weathered schists show yellowish and rusty colours. Very dense foliation is intensively folded. Foliation is defined by laminae composed of strongly elongated quartz and albite blasts, and of thin streaks and thicker laminae of muscovite deformed into the asymmetric kink folds (Fig. 6D). Within the quartz-albite laminae, quartz porphyroclasts and pyrite crystals are observed, as well as larger quartz-albite clasts with tails composed of muscovite with single chlorite flakes (Fig. 6E). In this schist variety, pyrite is much less abundant than in other schists from the Wieściszowice deposit. Pyrite forms small, rounded grains with numerous quartz inclusions, sometimes arranged parallel to the edges of pyrite grains (Fig. 6F).

Chlorite-albite-calcite schists (sample W5) were observed in the vicinity of an old adit. These schists are greyish-green with lighter, greenish spots. The constituents of rock: almost colourless chlorite, elongated calcite lenses and streaks of epidote, and titanite, are parallel arranged. Plagioclases, although almost completely transformed into albite, preserved not only the characteristic, microophitic texture but also the twinnings. Greenish spots are composed of calcite. Pyrite commonly forms clusters of several crystals (Fig. 7A) with strain fringes parallel to the foliation and composed of chlorite (Fig. 7B) and calcite (Fig. 7C).

Minerals and metamorphism of pyrite-bearing schists

Pyrite-bearing schists contain various proportions of quartz, plagioclase (albite), white mica and chlorite. Each of

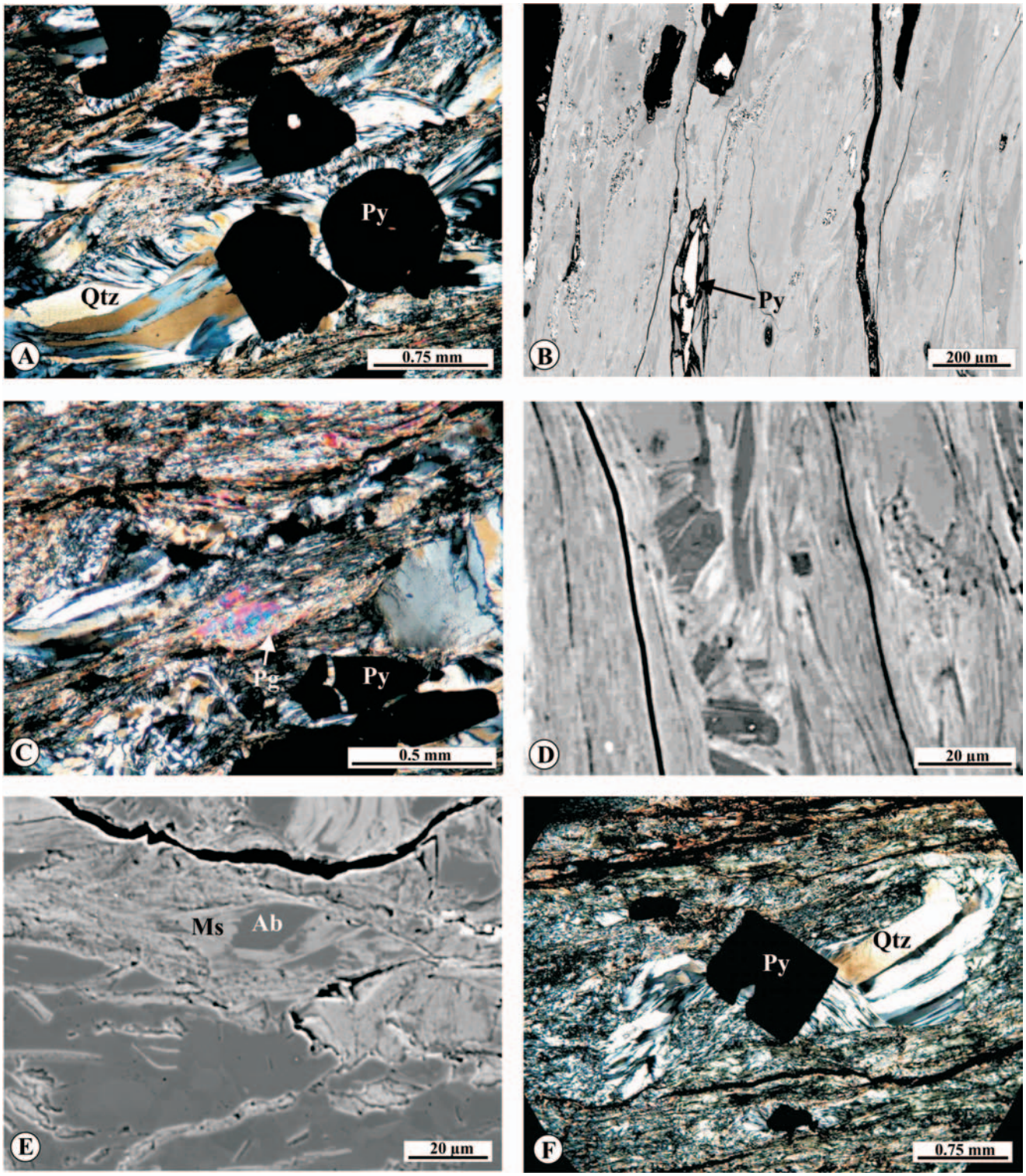

Fig. 5. **A** – sample W2, large pyrite crystals with strain fringes, section parallel to lineation, crossed polars; **B** – sample W2, Na-K mica (lighter streaks) intergrown with chlorite (darker streaks); strongly elongated pyrite crystals arranged parallel to mica-chlorite boundaries, BSE image; **C** – sample W2, paragonite-muscovite mica flake with fringed terminations enriched in K embedded within fine-grained fabric composed of light mica, chlorite, albite and titanite, section parallel to lineation, crossed polars; **D** – sample W 2, intergrowths of muscovite (light) and chlorite (dark) arranged obliquely to the flakes of older chlorite and light, paragonite-muscovite mica, BSE image; **E** – sample W 3, albite from the matrix overgrown with muscovite, BSE image; **F** – sample W 3, pyrite crystal with strain fringes in fine-grained matrix composed of chlorite, muscovite and elongated crystals of albite and quartz, section parallel to lineation, crossed polars. Ab – albite, Ms – muscovite, Pg – paragonite, Py – pyrite, Qtz – quartz

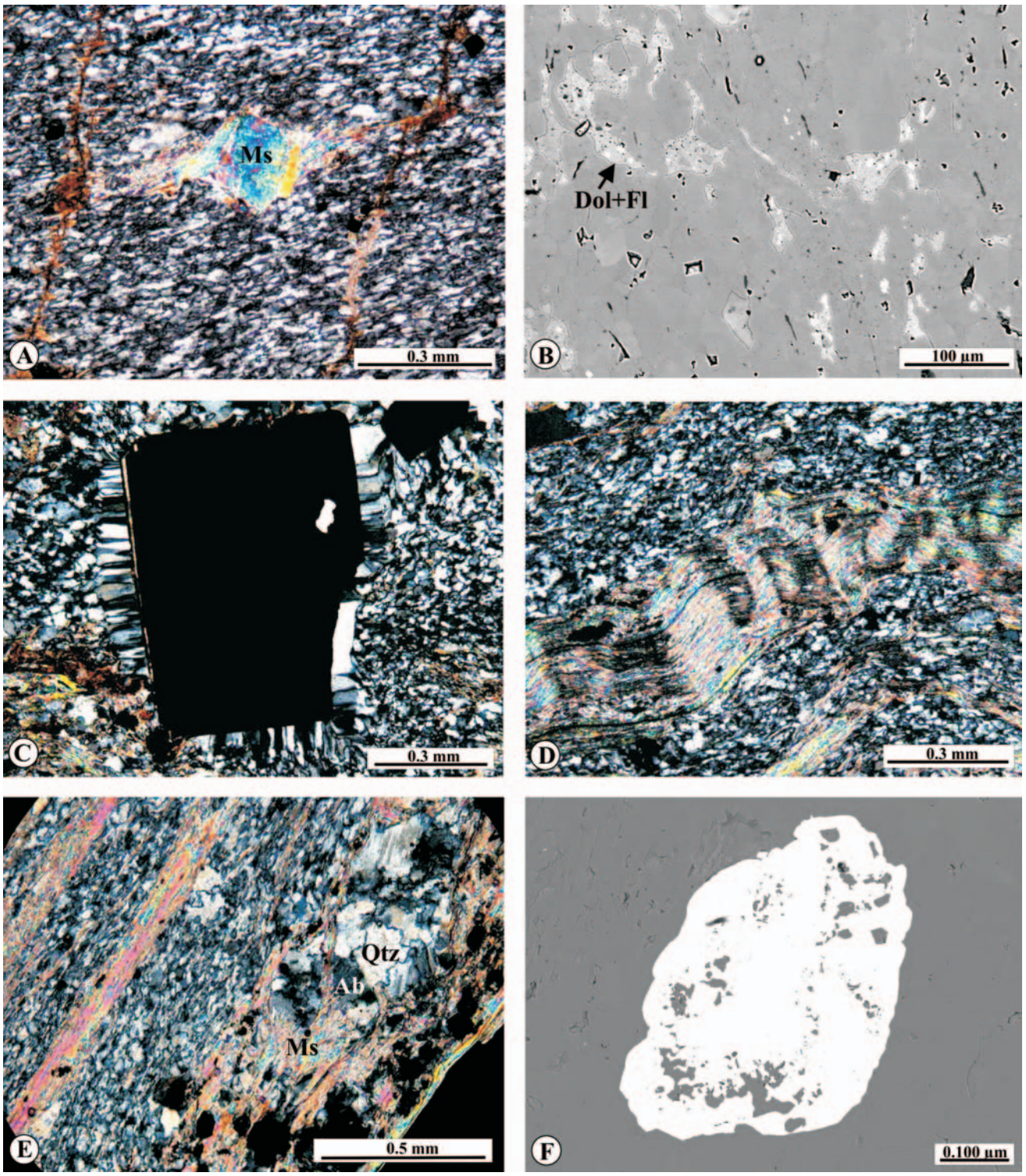

Fig. 6. **A** – sample W4, rotated muscovite clast with distinct tails in matrix composed of elongated albite, quartz and muscovite crystals, on the left – dolomite veinlet filling crack, section parallel to lineation, crossed polars; **B** – sample W4, amoebic "spots" of dolomite with minute fluorite inclusions (lighter spots) within quartz, BSE image; **C** – sample W4, pyrite crystal with short fringes embedded within matrix composed of isometric quartz and albite grains, section perpendicular to lineation, crossed polars; **D** – sample W1, muscovite laminae folded into asymmetric kink-folds, crossed polars; **E** – sample W1, quartz-albite clast with tails composed of muscovite and single chlorite crystals, crossed polars; **F** – sample W1, rounded pyrite crystal with quartz intergrowths distributed parallel to crystal edges, BSE image. Ab – albite, Dol – dolomite, Fl – fluorite, Ms – muscovite, Py – pyrite, Qtz – quartz

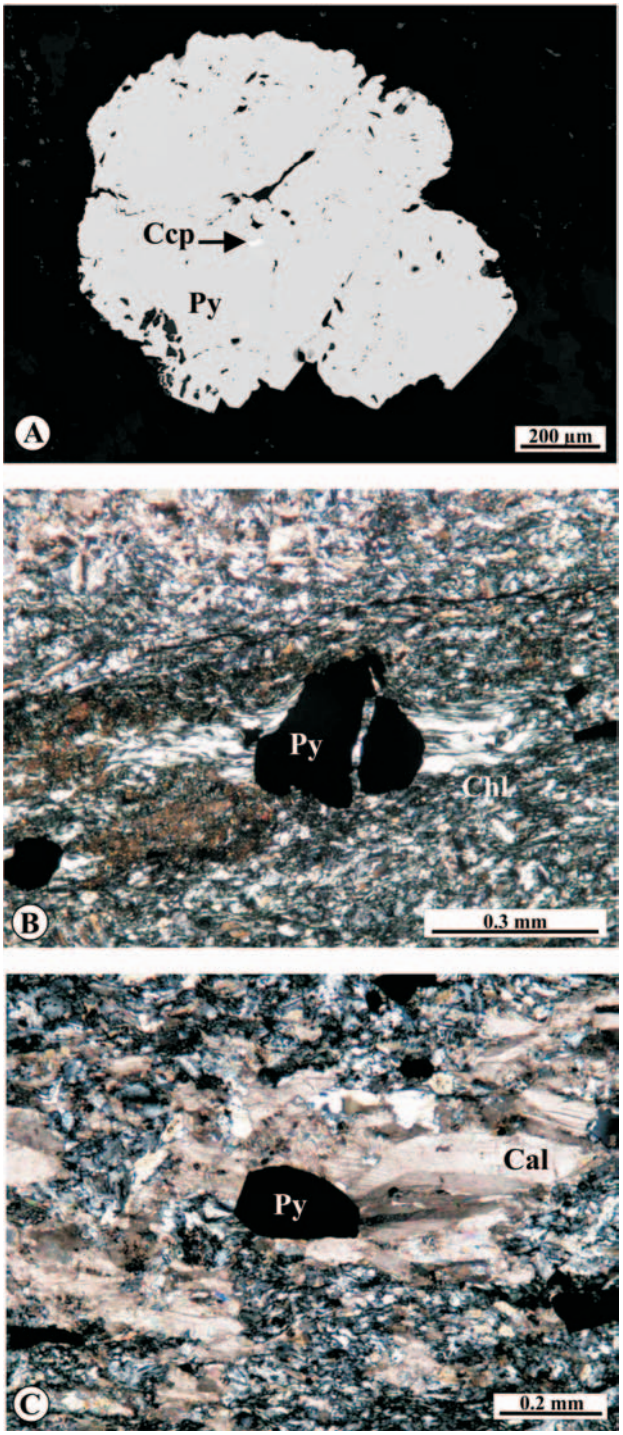

Fig. 7. **A** – sample W5, aggregate composed of several pyrite crystals with chalcopyrite inclusion, BSE image; **B** – sample W5, disrupted pyrite crystal with chlorite fringes arranged parallel to foliation. Crack in pyrite crystal filled with chlorite, crossed polars; **C** – sample W5, pyrite crystal with calcite fringes arranged parallel to foliation, crossed polars. Cal – calcite, Ccp – chalcopyrite, Chl – chlorite, Py – pyrite

these minerals is represented by at least two generations. Quartz forms small grains in the matrix and fibrous crystals composing fringes around pyrite grains. Plagioclase forms small grains in the matrix and larger, probably detrital clasts. Both generations of plagioclase are nearly pure albite.

Chlorite

All investigated chlorite grains (Table 3) belong to the type I ($x_{Mg}+x_{Fe} \geq x_{Al}+x_{\square}$) and to Mg-chlorites (Zane & Weiss, 1998). The average Fe/(Fe+Mg) ratio for chlorite grains is 0.165 (W1), 0.07 (W2), 0.35 (W3) and 0.28 (W5) (Table 3). The content of aluminum in tetrahedral Al^{IV} site ranges from 2.39 a.p.f.u. (atoms per formula unit) for sample W5 to 2.61 a.p.f.u. for sample W3.

The chemical variability of chlorites correlates well with the chemical composition of the host rocks (Tables 3, 4). The older generation of chlorite in the matrix and younger generation of chlorite forming the fringes around pyrite and filling the fractures in pyrite grains have the same chemical compositions when observed in the same thin section. This may suggest that the chemical composition of chlorites is controlled mostly by the chemical composition of the host rocks (Xie *et al.*, 1997; Zane *et al.*, 1998). However, it may also suggest that the metamorphic conditions during the crystallization of both the younger and the older chlorites were similar.

White mica

The schists observed in W1 and W3 samples contain muscovite with paragonite admixture (Fig. 8; Giorgetti *et al.*, 2003). The Na/(Na + K) ratio ranging from 0.07 to 0.33 (Figs 8A, 8B) is close to values found in natural muscovite (Guidotti & Sassi, 1998). The higher Na/(Na + K) ratio was found in white mica plates located close to albite grains. The Si content ranges from 6.16 to 6.32 a.p.f.u. in sample W1 and from 6.23 to 6.50 a.p.f.u. in sample W3. The highest value of Si (6.50 a.p.f.u.) was detected in a muscovite grain, which crystallized in the strain shadow near an albite porphyroclast. In sample W3 both the Fe and Mg contents are high (Fe 0.13 to 0.21 a.p.f.u. and Mg 0.23 to 0.35 a.p.f.u.), indicating that mica grains include a celadonitic component. The Fe content (0.05 to 0.12 a.p.f.u.) in muscovite from sample W1 is lower than in sample W3, but Mg content in W1 mica (0.2–0.34 a.p.f.u.) is similar to that in sample W3.

The white micas from sample W4 are characterized by Si concentrations ranging from 5.99 to 6.48 a.p.f.u. The Na/(Na + K) ratio varies from 0.11 (muscovite) to 0.98 (paragonite) (Fig. 8C). The Fe contents are low (<0.07), but Mg contents vary from 0.03 to 0.41 a.p.f.u. The lowest Mg values were detected in micas with the highest Na/(Na + K) ratios. In sample W4, the K-rich white mica forms rotated porphyroclasts (Fig. 6A, 8C). The mica fringes around these porphyroclasts contain more or less potassium than the porphyroclasts themselves. The Na-rich, white micas form small plates in the matrix. The same grain of mica commonly shows the muscovite composition at one analytical point and paragonite composition at the other. Such variability of white mica composition may be interpreted as discrete intergrowths of muscovite with paragonite, which cannot be detected with the EMP analysis (Livi *et al.*, 2008).

The schist from W2 sample contains compositionally variable white micas (Table 5). Their chemical compositions cover a full range from muscovite to paragonite. The Na/(Na + K) ratio ranges from 0.97 to 0.16. The highest Na/(Na + K) ratio was detected in a rotated porphyroclast of

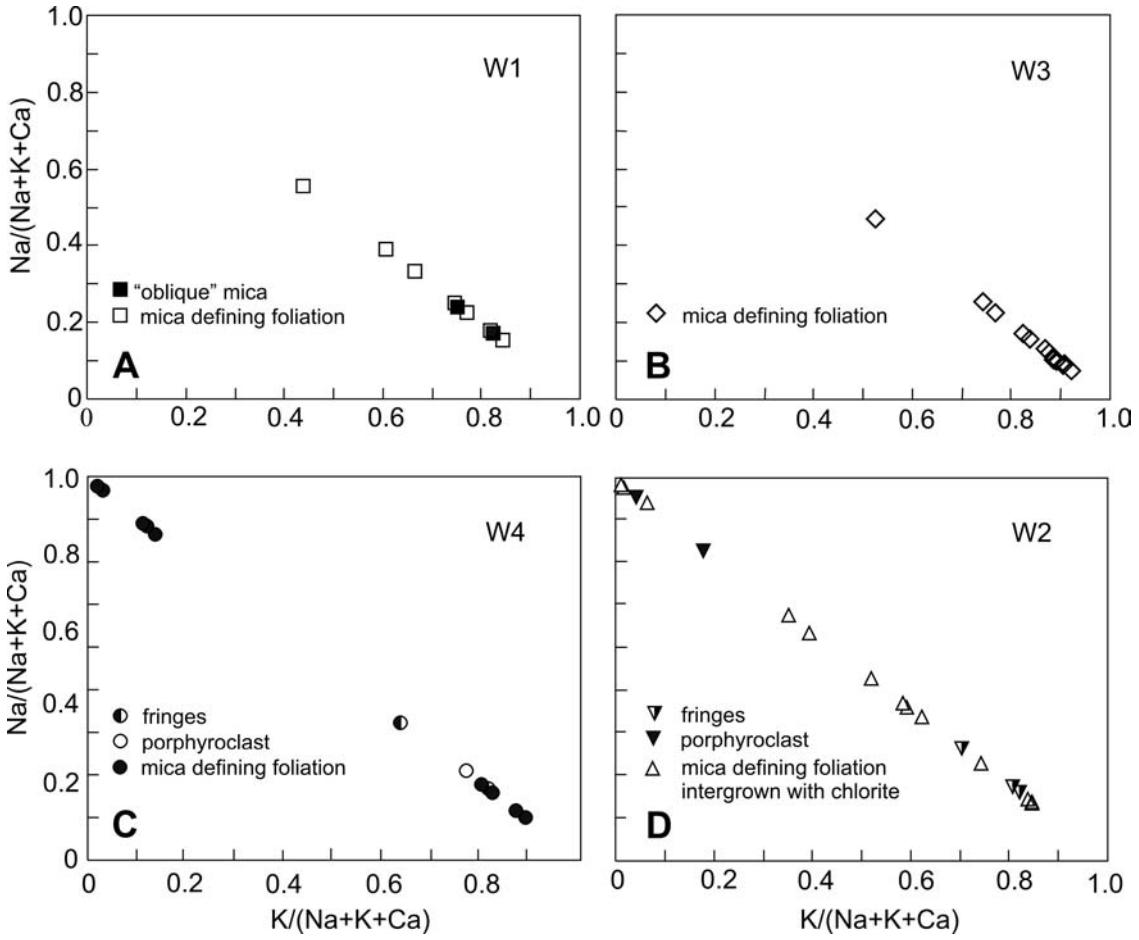

Fig. 8. Interlayer composition of white mica from the Wieściszowice pyrite-bearing schists

paragonite (Figs 5C, 8D) and in some small grains contained in white mica-chlorite packets (Fig. 5B). The other mica grains intergrown with chlorite and defining the foliation, the grains oblique to foliation and the grains forming fringes around paragonite porphyroclast, all show intermediate and low values of Na/(Na+K) ratio (Fig. 8D). The Si contents range from 6.02 to 6.40 a.p.f.u., the Fe contents are very low (Fe <0.01 a.p.f.u.) in paragonite and higher (Fe up to 0.07 a.p.f.u.) in muscovite. The Mg contents range from 0.02 a.p.f.u. in paragonite up to 0.49 in muscovite intergrown with chlorite.

The Ca content in all white micas is low and ranges from 0.001 to 0.018 a.p.f.u., and does not substantially change the interlayer sums.

Apart from the EMP analysis, an additional analysis of white mica was made using the XRD. Analysed material was selected from partly separated mica-rich domains encountered in the W2 sample. The X-ray diffraction pattern (Fig. 9) confirmed the presence of paragonite (d_{002} = 9.617 Å) and muscovite (d_{002} = 9.911 Å), and showed also distinct peaks of quartz, albite, chlorite and pyrite.

The comparison of chemical analyses of the Wieściszowice schists (Table 4) with chemical compositions of white mica in the particular varieties of schists shows that there is no simple dependence between the rock bulk composition and the chemistry of micas. The mica composition seems to be controlled by coexisting Na and Al phases, such as albite and chlorite, rather than by the rock bulk composition (Guidotii & Sassi, 1998). Paragonite coexists with muscovite in both the W4 and W2 schists. In sample W2, muscovite and paragonite occur together with intermediate Na-K micas. The intermediate Na-K micas form very small grains intergrown with chlorite (Fig. 5B, Table 5). Such intergrowths may form by hydrotermal alteration of the sea-floor deposits (Honnorez, 2003) and may represent metastable phases preserved during the regional metamorphism (Giorgetti *et al.*, 2003). In sample W4, paragonite is separated from muscovite by a wide immiscibility gap, with characteristic asymmetry towards the paragonite caused by higher solubility of Na in muscovite than that of K in paragonite (Roux & Hovis, 1996). Such an immiscibility gap is characteristic for micas formed under the regional metamorphic conditions (Giorgetti *et al.*, 2003). The occurrence of metastable phases in sample W2 and an immiscibility gap separating paragonite and muscovite in sample W4 may indicate that temperatures of metamorphism were similar to those of hydrothermal alteration.

The youngest mica forming fringes around muscovite (sample W4) and paragonite (sample W2) porphyroclasts has muscovite composition, similarly as "oblique" mica. It means that paragonite, being older than muscovite, did not originate from its transformation.

Table 3

Selected electron microprobe analyses (in wt %) and structural formulae of chlorite from the Wieściszowice pyrite-bearing schists. Area II

	W1		W2		W3						W5						
SiO_2	28.52	27.08	29.40	29.32	26.56	26.59	26.72	26.49	26.41	26.79	26.9	27.86	27.92	27.84	27.04	27.82	27.58
TiO_2	0.06	0.06	0.04	0.06	0	0.08	0.09	0.02	0	0.04	0.09	0.05	0	0	0	0.02	0.04
Al_2O_3	22.49	21.95	23.73	23.57	22.56	22.21	22.03	22.05	22.07	22.19	22.37	20.89	21.39	21.63	22.59	20.80	22.10
Cr_2O_3	0.02	0	0.01	0.04	0	0	0.03	0	0	0.04	0.23	0	0	0.02	0.17	0	0.02
MgO	26.47	24.94	29.86	29.92	19.80	19.15	20.26	20.05	19.53	19.55	20.93	22.00	21.54	21.67	21.48	21.93	21.56
CaO	0.05	0.06	0.02	0.03	0.04	0	0	0	0.04	0.04	0.05	0.12	0.06	0	0.05	0.02	0.05
MnO	0.20	0.11	0.20	0.23	0.13	0.10	0.29	0.11	0.19	0.13	0.81	0.79	0.82	0.96	0.72	1.01	0.87
FeO	8.90	8.94	3.80	4.03	18.31	19.29	18.48	17.99	19.04	18.66	15.83	15.07	15.92	14.84	15.13	15.26	15.49
Na_2O	0.02	0.02	0.04	0.02	0	0	0.01	0.01	0	0	0.02	0.01	0	0	0.01	0	0.02
K_2O	0	0	0.03	0.01	0	0	0	0	0	0	0.01	0	0	0.01	0	0	0
total	86.73	83.16	87.13	87.23	87.4	87.42	87.91	86.72	87.28	87.44	87.24	86.79	87.65	86.97	87.19	86.86	87.73
Numbers of ions on the basis of 28 O																	
Si	5.54	5.50	5.53	5.52	5.39	5.42	5.40	5.41	5.39	5.44	5.42	5.62	5.59	5.59	5.43	5.61	5.51
Al^{IV}	2.46	2.50	2.47	2.48	2.61	2.58	2.60	2.59	2.61	2.56	2.58	2.39	2.41	2.41	2.58	2.39	2.49
Al^{VI}	2.70	2.75	2.80	2.75	2.79	2.76	2.65	2.72	2.71	2.76	2.73	2.58	2.64	2.71	2.77	2.56	2.71
Ti	0.01	0.01	0.01	0.01	0	0.01	0.01	0	0	0.01	0.01	0.01	0	0	0	0	0.01
Cr	0	0	0	0.01	0	0	0.01	0	0	0.01	0.04	0	0	0	0.03	0	0
Fe	1.45	1.52	0.60	0.63	3.11	3.29	3.13	3.07	3.25	3.17	2.67	2.54	2.67	2.49	2.54	2.57	2.59
Mn	0.03	0.02	0.03	0.04	0.02	0.02	0.05	0.02	0.03	0.02	0.14	0.13	0.14	0.16	0.12	0.17	0.15
Mg	7.67	7.55	8.38	8.40	5.99	5.82	6.11	6.11	5.95	5.92	6.29	6.61	6.43	6.49	6.42	6.60	6.42
Ca	0.01	0.01	0.01	0.01	0.01	0	0	0	0.01	0.01	0.01	0.03	0.01	0	0.01	0	0.01
Na	0.01	0.01	0.02	0.01	0	0	0	0	0	0	0.01	0	0	0	0.01	0	0.01
K	0	0	0.01	0	0	0	0	0	0	0	0	0	0	0	0	0	0
XFe	0.16	0.17	0.07	0.07	0.34	0.36	0.34	0.33	0.35	0.35	0.29	0.27	0.29	0.27	0.28	0.28	0.28
S VI	11.86	11.85	11.82	11.84	11.91	11.90	11.96	11.92	11.94	11.89	11.88	11.87	11.88	11.85	11.88	11.90	11.88

W1 – muscovite-quartz-albite schists; W2 – chlorite-muscovite-(paragonite)-albite schists; W3 – chlorite-albite-quartz-muscovite schists; W5 – chlorite-albite-calcite schists

Metamorphic conditions of pyrite-bearing schists

The temperature of metamorphism which affected the Wieściszowice pyrite-bearing schists was estimated basing on the average chemical composition of chlorites from samples W3 and W5, using the Cathelineau method (1988), modified by Xie *et al.* (1997). Chlorite in sample W3 formed at temperature around 350°C, whereas that from sample W5 crystallized at *ca.* 340°C. Thus, the formation temperature of the Wieściszowice pyrite-bearing schists was about 340–350°C.

Characterization of disseminated mineralization in pyrite-bearing schists

In the schists from Wieściszowice, pyrite usually forms crystals of size from some tens of micrometres up to several millimetres. Pyrite crystals are *rounded* (W1; Figs 6F, 10A), *cuboidal* (W4, Fig. 6C; W3, Figs 5F, 10B; W2, Figs 5A, 10D) or form *intergrowths* (W5, Fig. 7A). The chemical composition of pyrite crystals is very consistent. Even the rims displayed at the back-scattered electron (BSE) images, which may reflect the effects of weathering, do not differ in composition from the inner parts of crystals. Pyrite crystals contain rare, euhedral chalcopyrite (sample W3, Fig. 10B) or single, quartz-monazite (W4) inclusions.

Pyrite crystals in sample W5 and W1 bear the signs of corrosion along the crystal edges and have minute cracks inside the crystals. In sample W5 pyrite crystals show irregular, shredded edges with hollows filled with calcite (Fig. 7A), whereas in sample W1 corrosion caused rounding of pyrite crystals (Fig. 6F) and rims of hollows filled with quartz were formed parallel to the edges of pyrite crystals. In such hollows rare, submicroscopic grains of chalcopyrite and galena were observed. Such submicroscopic grains as well as minute grains of chalcopyrite and tennantite accompanying pyrite clusters (Fig 10A), together with rows of tennantite crystals penetrating the fracture in pyrite crystal (sample W2; Fig 10D), are presumably the members of a younger assemblage of ore minerals related to the penetration of hydrothermal fluids, which corroded pyrite crystals. Such fluids might have precipitated not only quartz, which fills the ”hollows”, but also dolomite and fluorite (sample W4) and calcite (sample W5). Euhedral inclusions of chal-

Table 4

Chemical analyses of metamorphic rocks from areas I - Jarkowice and II - Wieściszowice

	Metabasites			Pyrite-bearing rocks from Wieściszowice					
wt%	J1	W7	W6	W5a	W5b	W4	W3	W2	W1
SiO_2	49.60	53.81	48.04	42.60	42.05	58.22	60.79	49.70	68.89
TiO_2	1.382	1.253	1.708	0.494	0.493	0.766	0.257	0.856	0.43
Al_2O_3	13.98	11.95	13.39	17.46	14.93	15.07	12.18	21.58	15.50
Fe_2O_3	13.16	11.22	13.00	11.02	13.41	7.23	7.90	7.41	2.90
MnO	0.146	0.173	0.233	0.449	0.413	0.031	0.083	0.038	0.023
MgO	7.00	4.05	5.95	10.08	8.36	2.96	4.64	6.94	3.35
CaO	7.16	6.27	12.80	3.98	5.74	1.65	5.57	0.61	0.09
Na_2O	4.59	4.32	2.65	4.16	4.1	3.24	2.09	2.44	2.49
K_2O	0.16	0.14	0.29	0.07	0.11	1.04	0.23	1.51	1.52
P_2O_5	0.21	0.12	0.17	0.02	0.05	0.13	0.06	0.05	0.04
LOI	2.47	6.52	1.57	8.55	9.33	9.34	6.21	8.25	3.90
S	0.013	0.01	0.031	2.87	5.48	4.01	0.689	3.77	1.04
Total	99.85	99.82	99.8	98.87	98.99	99.68	100.00	99.39	99.14
ppm									
Cr	84	< 5	130	63	118	36	67	62	22
Ni	49	4	67	32	43	16	11	21	15
Co	43	25	48	22	18	22	15	12	22
Sc	41.6	29.7	35	37	34.1	31.5	26.9	41.9	22.1
V	312	289	299	289	246	102	149	305	104
Cu	4	12	74	16	17	21	133	257	24
Pb	< 3	< 3	< 3	< 3	4	9	< 3	< 3	< 3
Zn	25	108	78	225	165	17	28	54	137
Cd	1.6	1.1	1.1	1	1.6	0.6	0.8	1.4	< 0.5
Ge	2.1	1.1	1.8	0.8	0.6	< 0.5	1.2	0.6	< 0.5
W	10.2	11.5	51.7	5.8	14.2	51.3	36.8	31.2	63
Sb	0.5	0.5	1.3	0.4	0.4	0.4	0.6	6.9	1.1
As	< 0.5	2.6	1.6	7.3	4.8	10.8	11.4	112	8.5
Bi	< 0.1	< 0.1	< 0.1	0.3	0.2	< 0.1	0.1	0.1	0.1
Rb	< 1	1	5	< 1	< 1	17	5	30	29
Cs	< 0.1	0.3	1.4	0.2	< 0.1	1.4	1.4	1.5	1.2
Ba	19	20	23	15	16	204	731	786	721
Sr	188	24	188	136	98	147	132	156	96
Ga	17	15	19	16	14	18	13	26	13
Ta	0.23	0.16	1.28	0.08	0.18	1.37	0.57	1.1	2.08
Se	< 3	< 3	< 3	< 3	< 3	10	< 3	18	< 3
Nb	2	0.9	3.3	0.4	0.4	3	2	2.8	3.3
Hf	2.3	1.6	3.2	0.6	0.5	2.6	1.2	1.6	3.4
Zr	64	41	102	16	13	74	42	49	100
Y	31.1	30.3	45.5	8	8.1	31.4	15.2	18.2	24.1
Th	0.42	0.2	0.22	0.28	0.18	1.78	2.93	0.63	0.87
U	0.2	0.21	0.19	0.3	0.56	1.31	1.57	0.56	1.39
La	2.84	2.6	3.87	0.87	1.26	6.86	9.19	1.4	1.28
Ce	8.3	6.53	12.00	2.3	3.03	15.8	17.7	4.11	2.62
Pr	1.52	1.34	2.22	0.39	0.49	2.38	2.35	0.78	0.36
Nd	8.77	7.98	12.6	2.15	2.55	12.2	9.13	4.71	1.78
Sm	3	2.96	4.23	0.67	0.77	3.47	2.1	1.68	0.51
Eu	1.17	1.21	1.57	0.435	0.486	0.869	0.686	0.753	0.11
Gd	4.18	4.15	5.79	0.94	1.06	4.17	2.03	2.18	0.93
Tb	0.8	0.8	1.12	0.19	0.2	0.77	0.34	0.41	0.31
Dy	5.25	5.35	7.32	1.32	1.34	5.00	2.19	2.76	2.9
Ho	1.11	1.07	1.55	0.29	0.29	1.07	0.47	0.59	0.78
Er	3.46	3.07	4.65	0.9	0.94	3.26	1.46	1.84	2.86
Tm	0.534	0.46	0.7	0.138	0.145	0.497	0.223	0.296	0.5
Yb	3.31	2.8	4.34	0.9	0.94	3.21	1.44	1.89	3.43
Lu	0.468	0.397	0.605	0.133	0.143	0.503	0.219	0.271	0.549
ΣRRE	44.712	40.717	62.565	11.626	13.644	60.059	49.528	23.67	18.919
LaN/YbN	0.57	0.62	0.6	0.65	0.9	1.43	4.27	0.5	0.25
Eu/Eu*	1.02	1.06	0.98	1.68	1.65	0.7	1.02	1.21	0.49

Table 5

Electron microprobe analyses (in wt %) and structural formulae of white micas from chlorite-muscovite-(paragonite)-albite schists (sample W2). Area II - Wieściszowice

	Pg in matrix	White mica/chlorite packets*				White mica in matrix						Porphyroclast with fringed terminations**					oblique white mica ***	Chl/Ms inter-growths
SiO_2	48.98	48.65	49.13	48.46	49.14	49.8	48.17	47.93	47.9	47.75	47.75	48.59	48.06	47.55	47.8	47.93	48.05	48.95
TiO_2	0.00	0.00	0.04	0.12	0.09	0.05	0.10	0.11	0.16	0.22	0.30	0.10	0.09	0.05	0.04	0.09	0.08	0.06
Al_2O_3	38.74	40.52	41.65	38.43	37.83	37.41	36.41	34.72	33.46	33.81	33.44	33.41	35.05	39.86	39.04	33.51	36.14	34.23
Cr_2O_3	0.02	0.05	0.01	0.04	0.02	0.00	0.08	0.07	0.02	0.00	0.00	0.01	0.00	0.03	0.07	0.06	0.01	0.05
MgO	0.36	0.12	0.11	0.46	0.68	1.09	1.19	1.36	1.84	1.48	1.70	1.89	1.53	0.13	0.26	1.80	1.21	2.52
CaO	0.00	0.14	0.1	0.14	0.08	0.04	0.03	0.01	0.03	0.00	0.00	0.00	0.02	0.12	0.16	0.00	0.04	0.01
MnO	0.00	0.00	0.00	0.09	0.00	0.04	0.00	0.06	0.02	0.03	0.03	0.06	0.00	0.00	0.04	0.00	0.00	0.00
FeO	0.41	0.02	0.08	0.23	0.25	0.28	0.42	0.32	0.6	0.45	0.59	0.34	0.49	0.07	0.24	0.42	0.36	0.51
BaO	0.22	0.26	0.00	0.65	0.30	0.28	0.32	0.24	0.24	0.36	0.52	0.42	1.03	0.00	0.36	0.58	0.48	0.61
Na_2O	7.14	6.93	7.4	3.81	4.24	3.33	2.98	2.77	1.13	1.87	1.11	1.44	2.08	7.05	5.69	1.28	2.82	1.15
K_2O	0.74	0.18	0.14	3.85	3.55	5.51	6.41	6.91	9.57	8.30	9.24	9.18	7.57	0.48	1.89	8.88	6.30	9.03
total	96.61	96.86	98.66	96.27	96.17	97.82	96.11	94.49	94.96	94.26	94.67	95.44	95.93	95.33	95.57	94.55	95.49	97.12
Numbers of ions on the basis of 22 O																		
Si	6.16	6.07	6.02	6.18	6.25	6.28	6.23	6.31	6.36	6.35	6.36	6.4	6.29	6.04	6.1	6.37	6.25	6.34
Al^{IV}	1.84	1.93	1.98	1.82	1.76	1.73	1.77	1.69	1.64	1.65	1.65	1.60	1.71	1.96	1.90	1.63	1.75	1.66
Al^{VI}	3.91	4.03	4.03	3.95	3.91	3.83	3.77	3.7	3.59	3.65	3.6	3.59	3.69	4.01	3.97	3.62	3.79	3.57
Ti	0.00	0.00	0.00	0.01	0.01	0.01	0.01	0.01	0.02	0.02	0.03	0.01	0.01	0.01	0.00	0.01	0.01	0.01
Cr	0.00	0.01	0.00	0.00	0.00	0.00	0.01	0.01	0.00	0.00	0.00	0.00	0.00	0.00	0.01	0.01	0.00	0.01
Fe^{2+}	0.04	0.00	0.01	0.02	0.03	0.03	0.05	0.04	0.07	0.05	0.07	0.04	0.05	0.01	0.03	0.05	0.04	0.06
Mn	0.00	0.00	0.00	0.01	0.00	0.00	0.00	0.01	0.00	0.00	0.00	0.01	0.00	0.00	0.01	0.00	0.00	0.00
Mg	0.07	0.02	0.02	0.09	0.13	0.20	0.23	0.27	0.36	0.29	0.34	0.37	0.30	0.03	0.05	0.36	0.24	0.49
Ca	0.00	0.02	0.01	0.02	0.01	0.01	0.00	0.00	0.00	0.00	0.00	0.00	0.00	0.02	0.02	0.00	0.01	0.00
Ba	0.01	0.01	0.00	0.03	0.02	0.01	0.02	0.01	0.01	0.02	0.03	0.02	0.05	0.00	0.02	0.03	0.02	0.03
Na	1.74	1.68	1.76	0.94	1.04	0.82	0.75	0.71	0.29	0.48	0.29	0.37	0.53	1.74	1.41	0.33	0.71	0.29
K	0.12	0.03	0.02	0.63	0.58	0.89	1.06	1.16	1.62	1.41	1.57	1.54	1.26	0.08	0.31	1.51	1.04	1.49

*Fig. 5B; **Fig. 5C; ***Fig. 5D

copyrite in chlorite-rich schists (sample W5) (Fig. 7A) probably belong to the same sulphide assemblage. Their link cannot be neglected to crystal lattice failures in hosting pyrite grains, although such failures have not been observed in the vicinity of crystals shown in the photographs. The fact that "hollows" and fractures in pyrite crystals are filled with minerals observed in the matrix (quartz in sample W1, calcite in W5, chlorite, titanite and quartz in W3; Fig. 10C) and that the signs of As, Cu and Pb mineralization are scarce may suggest that elements forming this mineralization were leached from the host-rocks.

Microstructural timing of pyrite mineralization

In the pyrite-bearing schists outcropping at the abandoned mine in Wieściszowice, the penetrative foliation dips at 40 to 65° to the NE and east whereas the stretching lineation plunges to the north and NNE at low and moderate angles. The delicate mica lineation is oblique to it. The axes of older folds are parallel to the stretching lineation. The folds show different morphologies: from isoclinal and open forms to chevron-type folds developed in sample W1 schist. The younger folds are open structures, often fractured at hinges.

In thin sections cut parallel to the stretching lineation and perpendicular to the foliation, the kinematic indicators, such as asymmetric strain shadows (Figs 5C, 5E, 6A) and strain fringes around pyrite grains are visible.

In schists from samples W1, W2, W3 and W4, strain fringes are composed of several groups of fibrous quartz crystals connected with more or less visible sutures (Figs 5A, 5F). The strain fringes are absent or are very short in sections perpendicular to the lineation (Fig. 6C). The shapes of strain fringes and their arrangement suggest the non-coaxial type of deformation.

In chlorite-albite-calcite schists (W5) and, sometimes, also in chlorite-albite-quartz-muscovite schists (W3) the strain fringes are composed of fibrous chlorite (Fig. 7B) and calcite (Fig. 7C). In sample W5 fringes are parallel to the foliation. Such straight fringes are rare in the remaining varieties of the studied schists. It is accepted that straight fringes are concordant with the X direction of final strain (Passchier & Trouw, 2005).

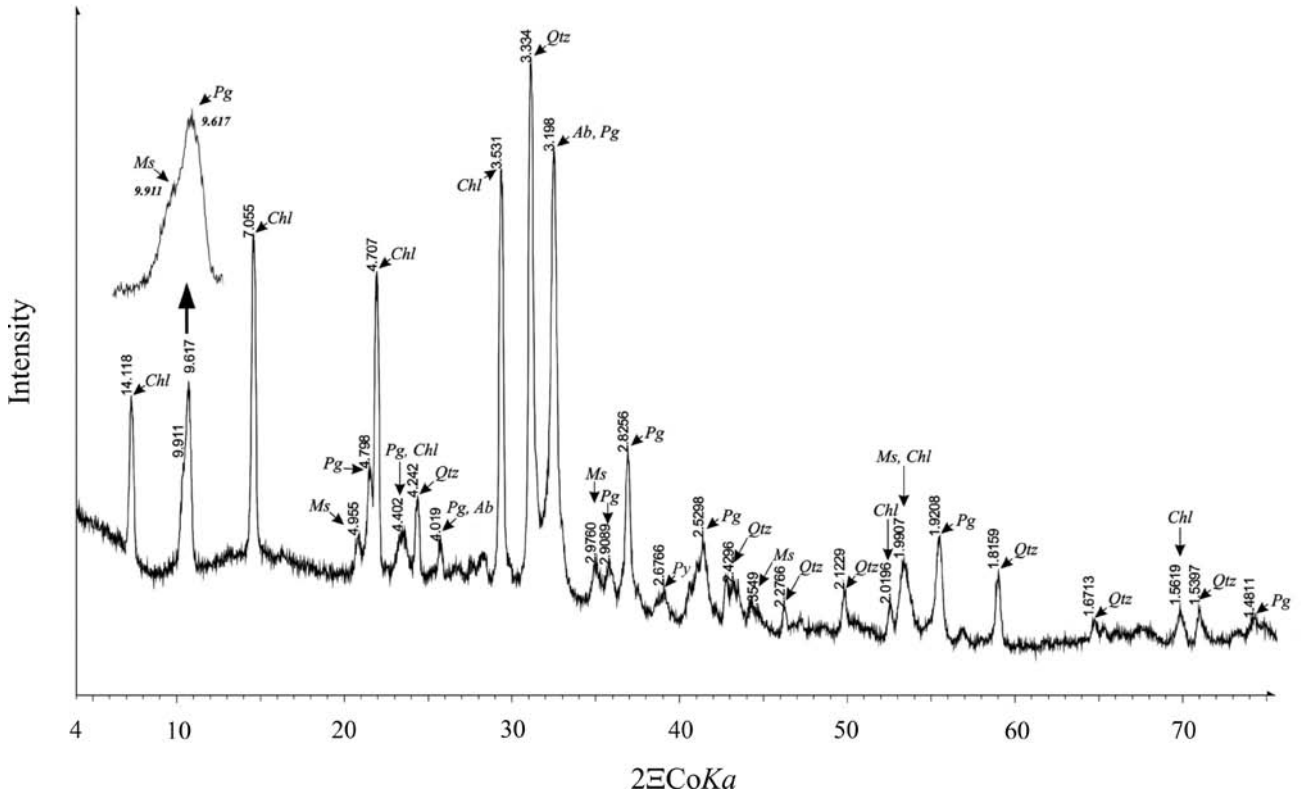

Fig. 9. XRD pattern of sample W2. Numbers above pattern are d-spacings in Å. Pg – paragonite, Qtz – quartz, Ms – muscovite, Ab – albite, Chl – chlorite

The pyrite crystals do not contain intergrowths of metamorphic minerals and the microstructural criteria do not allow definitive determination of age relationships between pyrite porphyroblasts, penetrative foliation and penetrative stretching lineation. The foliation and lineation, defined by the same mineral domains, were formed contemporaneously. The presence of strongly elongated pyrite crystals in packets of paragonite-muscovite micas and chlorite (Fig. 5B) demonstrates that at the very early stages of foliation and lineation development, pyrite did not form large, euhedral crystals. Their origin was probably connected with the recrystallization, which took place between the first and the second stages of foliation and lineation development. Kinematic indicators of shear reveal that the second stage of foliation and lineation took place under non-coaxial deformation conditions and simultaneous extension, indicated by the strong elongation of quartz and albite grains. During this deformation, pyrite crystals were rotated and bended strain fringes were formed. In schists from sample W4, the formation of fringes was preceded by crystallization of dolomite rims around pyrite crystals (Fig. 6C). The next deformation phase was coaxial. At the edges of pyrite crystals the straight fringes (W5) were formed, parallel to the stretching lineation. An independent proof for stretching is the presence of cracks in pyrite crystals (Figs 5C, 7B). During this late tensional stage the fluids were probably activated, which caused corrosion of pyrite crystals in schists from samples W1 and W5 (Figs 6F, 7A). These fluids were the source of accessory sulphides crystallizing in the cracks and "hollows" in pyrite (Figs 10D, 6F).

Re-Os isotopic age determinations of pyrite from Wieściszowice

Seven samples of pyrite separated from four samples of schists, labeled W2, W3, W4 and W5a, showing an obvious, schistose penetrative fabric and containing disseminated, euhedral crystals of pyrite, approximately 1–2 mm in size, were analysed. The Re contents were 4–30 ppb Re, suitable for Re-Os geochronology given the likely Palaeozoic age of the pyrite occurrences. The results are presented in Table 7.

Generally, the pyrite samples have low to very low common Os contents, and the Os is dominated by $^{187}Os^*$, radiogenic Os derived from ^{187}Re decay. As such, the measured $^{187}Os/^{188}Os$ ratios are high to exceptionally high. For the purposes of geochronology of such samples the best solution is to exclude ^{188}Os as a denominator as its precise quantification is highly uncertain. Six pyrite samples yielded Model Ages of ~ 480 Ma (W2 – 480 Ma, W2-2 – 466 Ma, W3 – 479 Ma, W3-2 – 484 Ma, W5a – 487 Ma, W5a-2 – 508 Ma), whereas sample W4 yielded an older Model Age of 524 Ma. These data were plotted on an isochron diagram in Fig. 11, which shows that samples W2, W3 and W5a form a regression having an indicated age of 469 ± 20 Ma (2σ, Model 2). Sample W4 plots well above this regression line (not shown). It is important to note that pyrite from sample W4 showed significant discolouration (tarnishment) and that completely fresh material could not be obtained.

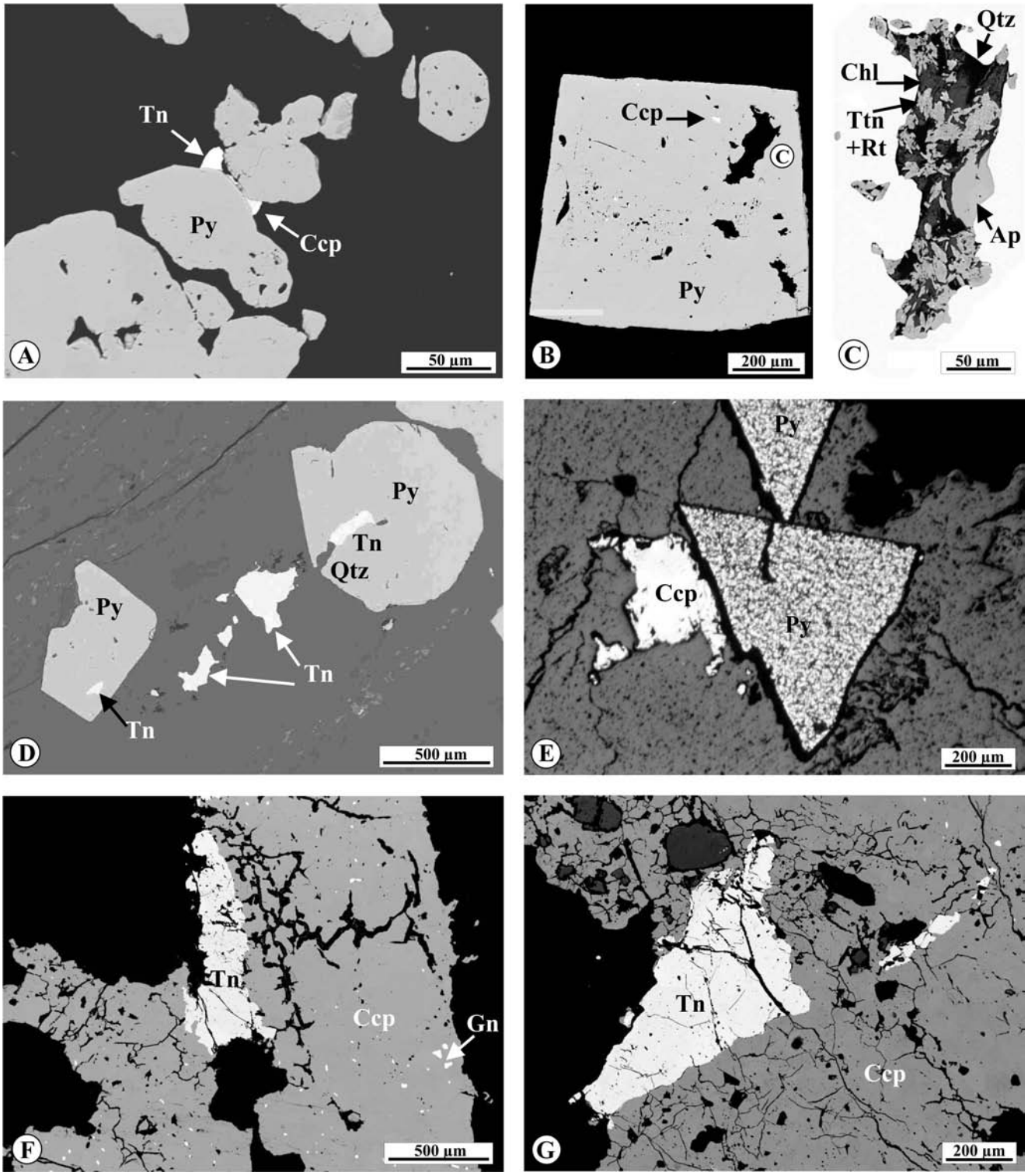

Fig. 10. A – sample W1, minute chalcopyrite and tennantite crystals scattered between pyrite aggregates, BSE image; **B** – sample W3, pyrite crystal with "hollows" and chalcopyrite inclusion, BSE image; **C** – sample W3, "hollow" seen in upper right corner of Fig. 10B filled with chlorite, titanite ("brushes") with rutile inclusions, and quartz, BSE image; **D** – sample W2, cracks in pyrite penetrated by younger tennantite and quartz, BSE image: **E** – quartz vein with euhedral pyrite crystals and adjacent chalcopyrite aggregate, reflected light; **F** – quartz vein with chalcopyrite-tennantite aggregate; chalcopyrite hosts minute galena intergrowths, BSE image; **G** – quartz vein with chalcopyrite-tennantite intergrowths, BSE image. Ap – apatite, Ccp – chalcopyrite, Chl – chlorite, Gn – galena, Py – pyrite, Qtz – quartz, Rt – rutile, Tnt – tennantite, Ttn – titanite

Table 6

Chemical composition and formulae of selected sulphides from the Wieściszowice pyrite deposit. Area II

Element	Pyrite	Chalcopyrite	Tennantite		Galena
Sample	Wb2, Wz4/7 n=14	Wb2, Wz4/7 n=16	Wb2 n=12	Wz4/7 n=13	Wz4/7 n=6
S	52.88	34.14	28.05	27.28	10.91
Fe	45.83	29.98	6.21	2.81	0.00
Cu	0.00	34.4	41.97	42.63	0.00
Zn	n.a.	0.02	1.43	5.21	0.00
As	0.02	0.03	19.43	18.66	0.00
Se	n.a.	0.00	0.20	0.11	3.93
Ag	0.00	0.03	0.04	0.15	0.06
Cd	0.00	0.02	0.12	0.57	0.07
Sb	0.01	0.01	1.08	2.89	0.00
Te	n.a.	0.04	0.26	0.03	0.07
Pb	n.a.	0.00	0.00	0.00	83.65
Bi	n.a.	0.00	0.01	0.00	0.00
Co	0.05	n.a.	n.a.	n.a.	n.a.
Ni	0.03	n.a.	n.a.	n.a.	n.a.
Total	98.79	98.67	98.80	100.35	100.42
Numer of ions (a.p.f.u.)					
S	2.006	1.973	12.947	12.457	0.84
Fe	0.998	0.995	1.646	0.736	0.00
Cu	0.00	1.003	9.774	9.825	0.00
Zn	n.a.	0.001	0.323	1.167	0.00
As	0.00	0.001	3.838	3.648	0.00
Se	n.a.	0.00	0.038	0.021	0.123
Ag	0.00	0.001	0.006	0.02	0.001
Cd	0.00	0.00	0.016	0.074	0.002
Sb	0.00	0.00	0.131	0.348	0.00
Te	n.a.	0.001	0.031	0.004	0.001
Pb	n.a.	0.00	0.00	0.00	0.997
Bi	n.a.	0.00	0.001	0.00	0.00
Co	0.001	n.a.	n.a.	n.a.	n.a.
Ni	0.001	n.a.	n.a.	n.a.	n.a.

n.a. – not analysed

Ore mineralization in quartz veins cutting pyrite-bearing schists

The quartz veins with calcite and green fluorite cutting through the schists in the Wieściszowice pyrite deposit were already mentioned by Berg (1938). Jaskólski (1964) reported on numerous veins of milky and white quartz, commonly with feldspars, for which he proposed the name "dry Alpine veins". Later on, Piestrzyński and Salamon (1977) described quartz veins with carbonates, sulphides and sulphosalts. These authors distinguished three stages of vein formation. At the first stage quartz, pyrite and pyrrhotite have crystallized, followed by the second-stage assemblage of chalcopyrite, sphalerite, galena, tetrahedrite and siderite, and by the third-stage assemblage of bournonite, jamesonite, boulangerite, galena, calcite and dolomite.

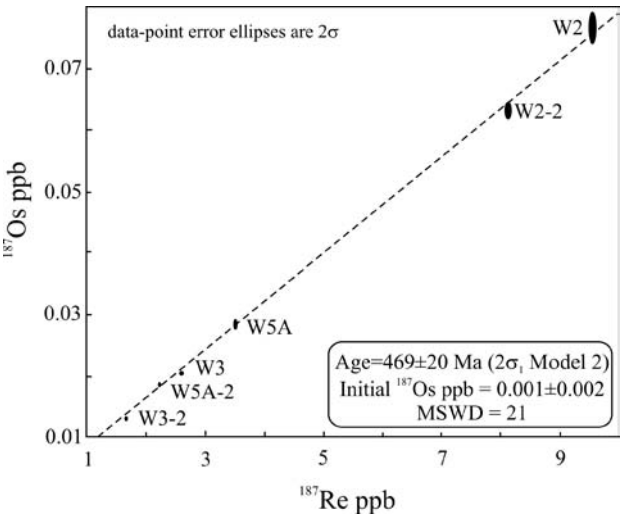

Fig. 11. Re-Os isochron diagram for pyrite separates

During the field work, mostly the barren quartz veins were encountered in the open pit. However, close to the north-eastern corner of the open pit the quartz veins were found, up to several tens of centimetres thick, which hosted large aggregates of sulphides. The veins were composed of milky quartz, sometimes cut by cracks filled with limonite. Occasionally, the relics of surrounding schists were present with disseminated pyrite and Ti minerals. Some pyrite crystals were strongly cracked and contained inclusions of gangues and chalcopyrite. Commonly, chalcopyrite rimmed or cemented pyrite crystals (Table 6; Fig. 10E).

Larger chalcopyrite accumulations were found in the milky quartz as nests of diameter up to several millimetres. An euhedral pyrite inclusion was found in chalcopyrite in a single polished section. Chalcopyrite aggregates host very fine, randomly disseminated galena crystals (Figs 10F, 10G). In the same sections, chalcopyrite intergrowths with tennantite were noticed (Table 6; Figs 10F, 10G).

The sulphide assemblage from the quartz veins is identical with that known from the schists (pyrite, chalcopyrite, galena), but proportions between sulphides are different – the mineralization in veins is dominated by chalcopyrite, whereas pyrite occurs in small amounts and is related to schist relics. These observations suggest that mineralization in quartz veins originated from the action of hydrothermal fluids, which remobilized metals from the pyrite-bearing schists. Such origin of the ore minerals vein is different from that described by Piestrzyński and Salamon (1977), as veins encountered by our team host different mineral paragenesis.

Formation temperature of quartz veins

The formation temperature of quartz veins was determined with the fluid inclusions (FI) microscopic studies carried on with the heating-freezing stage. The sample of milky quartz for measurements was selected from a vein with macroscopically visible chalcopyrite aggregates. Three

Table 7

Re-Os isotopic results for pyrite from the Wieściszowice pyrite deposit. Area II

Sample	Re (ppb)	^{187}Re (ppb)	^{187}Re/^{188}Os[1]	^{187}Os*[2] (ppb)	^{187}Os/^{188}Os[3]	Model Age (Ma)[4]
W2	15.195 ± 0.064	9.550 ± 0.041		0.0767 ± 0.0020	2093	480
W2-2	12.926 ± 0.055	8.124 ± 0.035		0.0633 ± 0.0010	4268	466
W3	4.139 ± 0.019	2.602 ± 0.012	780.2	0.0208 ± 0.0002	6.38	479
W3-2	2.653 ± 0.014	1.667 ± 0.009	628.1	0.0135 ± 0.0002	5.201	484
W4	27.792 ± 0.118	17.468 ± 0.074		0.1531 ± 0.0011	146.8	524
W5A	5.595 ± 0.025	3.516± 0.016		0.0287 ± 0.0006	70.12	487
W5A-2	3.561 ± 0.016	2.238 ± 0.010		0.0190 ± 0.0002	28.5	508

[1]– reported only if ^{187}Re/^{188}Os ratio <5,000; [2] – radiogenic ^{187}Os (^{187}Os*) reported for samples with calculated ^{187}Re/^{188}Os ratios >5,000, assuming common Os has an initial ^{187}Re/^{188}Os ratio of 0.12; [3] – measured ^{187}Re/^{188}Os ratios corrected for spike and mass fractionation. Uncertainties are mostly <1% 2SE; [4] – Model Age assumes an initial ^{187}Re/^{188}Os ratio of 0.12

types of inclusions were identified: type 1 (T1) and type 2 (T2) are primary inclusions, and type 3 (T3) includes secondary inclusions.

The T1 inclusions are large (over 20 μm across), single or forming groups of three or four individuals, generally irregular, but also oval or imitating the crystal habit of the hosting mineral. The inclusions are two-phase (V+L) or three-phase (L1+L2+V), rich in gaseous components (liquid and gaseous carbon dioxide and water). Gaseous phase occupies from 30 to 70% of the inclusion volume.

The T2 inclusions are usually less than a dozen of micrometres in diameter. These form random groups composed of several individuals or are distributed at crystal growth planes. The T2 inclusions are two-phase, H_2O-CO_2, with gaseous phase constituting 20% of the inclusion volume.

The T3 inclusions are small (several, rarely a dozen of micrometres), one or two-phase, arranged in rows or covering larger surfaces of cracks within the crystals.

The T1 inclusions showed melting temperatures of solid CO_2 from –58 to –66°C. The temperature decrease suggests presence of methane. Ice melted completely at about –2°C. Gas hydrate dissolved at temperatures between 8 and 14.9°C. Homogenization of CO_2 towards the gaseous phase occurred at temperatures between 22 and 30.6°C. The observed complete homogenization took place at temperatures from 335 to 377°C. Homogenization towards the gaseous phase was observed in a single inclusion at a temperature of 335°C.

The T2 inclusions revealed ice melting at the temperature range from –6 to 0°C. Rarely, the gas hydrate in these inclusions melted at about 6°C. Complete homogenization took place at the temperature range from 120 to 234°C.

The T3 inclusions showed the lowest homogenization temperatures: from 85 to 175°C. The lowest recorded ice melting temperature was –22°C, but in most of T3 inclusions it occurred at higher temperatures: from –16 to about –3°C.

The results of FI studies enable us to conclude that crystallization of milky quartz from veins cutting the Wieściszowice deposit took place at temperature range from 377 to 85°C.

Geochemistry of ore minerals from the Area II - Wieściszowice

The EMP analyses were carried on for pyrite, chalcopyrite and tennantite crystals from disseminated mineralization in the schists (sample Wb2) and from the quartz veins (sample Wz4/7). Galena sampled in the quartz veins was analysed as well.

Both pyrite and chalcopyrite show chemical compositions close to the stoichiometric ones. No significant admixtures were detected as all analysed trace elements occurred at the level of 0.00X wt.%. No differences were found in composition of sulphides from disseminated and vein mineralization except for galena and tennantite. Galena from quartz veins, found as inclusions in chalcopyrite, contained higher amounts of Se (3.93 wt.%). Tennantite from disseminated mineralization (sample Wb2) revealed higher contents of Fe (6.21 wt.%), Se (0.2 wt.%) and Te (0.26 wt.%), whereas tennantite from quartz veins (sample Wz4 and Wz7) contained higher amounts of Zn (5.21 wt.%), Cd (0.57 wt.%), Ag (0.15 wt.%) and Sb (2.89 wt.%) (Table 6).

The similarity in chemical compositions of the ore minerals representing disseminated mineralization and mineralization of quartz veins confirms our opinion that mineralization in quartz veins resulted from the action of hydrothermal fluids originating from metamorphic processes.

GEOCHEMISTRY OF ROCKS FROM THE AREA I - JARKOWICE AND THE AREA II - WIEŚCISZOWICE

The results of the whole rock chemical analyses of streaky amphibolite (J1) from Jarkowice magnetite site, two amphibolite samples from the quarry west of Wieściszowice village (samples W6 and W7), and six samples of pyrite-bearing schists from the Wieściszowice open pit (samples W1, W2, W3, W4, W5a and W5b) are listed in Table 4.

Major elements. Taking into account the contents of SiO_2, all analysed rocks can be divided into the two groups. The first group includes samples: J1, W7, W6, W5a, W5b

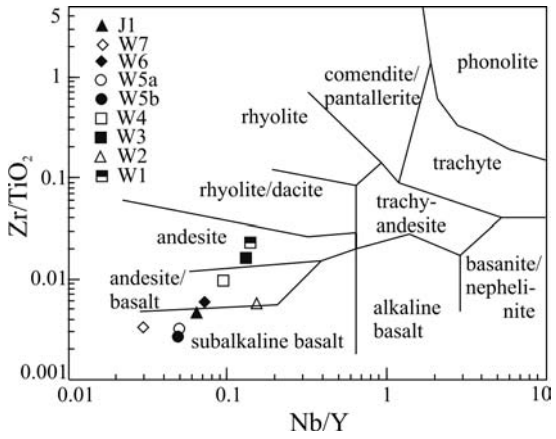

Fig. 12. Wieściszowice pyrite-bearing schists plotted on Nb/Y-Zr/TiO_2 diagram (Winchester & Floyd, 1977)

and W2, where SiO_2 contents are below 50 wt.% (except *ca*. 54 wt.% in sample W7). The SiO_2 content is higher in the remaining three samples (Table 4). The Fe_2O_3 contents are higher (11.02 to 13.41 wt.%) in samples J1, W7, W6, W5a and W5b, but do not exceed 7.9 wt.% in the remaining samples (Table 4). It must be emphasized that no positive correlation was found between the contents of Fe_2O_3 and S. On the contrary, samples with low Fe_2O_3 content usually contained more sulphur, which proves the lack of correlation between the contents of Fe and pyrite. Significant differences between amounts of CaO in samples W5a and W5b, collected some tens of centimetres apart suggest that Ca derived from decomposition of plagioclases (microophitic structure) might have migrated at short distances, probably in relation to crystallization of calcite. However, as the Na content in both samples is identical, it cannot be precluded that different contents of Ca resulted not from migration, but rather from local accumulations of Ca-bearing minerals – *e.g*., pyroxene – in the protolith of chlorite-albite-calcite schists. Such enrichment may suggest magmatic segregation. Attention should be paid also to high contents of K_2O in the following samples: W2 – 1.51 wt.%, W1 – 1.52 wt.% and W4 – 1.04 wt.%; in comparison with samples W5a – 0.07 wt%, W5b – 0.11 wt% and W3 – 0.23 wt%. Moreover, samples W2, W1 and W4 contained relatively high amounts of Na_2O, *i.e*. 2.44, 2.49 and 3.24 wt.%, respectively. A relatively high content of Na_2O (2.09 wt.%) was also determined in chlorite-albite-quartz-muscovite schist from sample W3.

Contents of main elements are reflected in mineral composition of studied rocks expressed in their names. It should be noticed that the presence of Na in these samples means the existence of albite, but, in samples W2 and W4, it also means the existence of paragonite (precisely, Na-K mica).

All samples plotted in the Zr/TiO_2 vs. Nb/Y diagram (Fig. 12; Winchester & Floyd, 1977) belong to the subalkaline basalt, andesite/basalt and andesite fields.

Trace elements. Among studied samples, the J1, W6, W7 and W2 samples reveal very similar geochemical signature of trace elements. In these four samples (particularly in W2), the highest variability of trace elements contents was observed, particularly among the incompatible elements (Fig. 13A). Generally, the Nb anomaly is poorly marked, whereas Ti and P anomalies are absent and Sr anomaly occurs only in sample W6. The compatible elements from Sm to Yb reveal rather monotonous pattern (almost horizontal in sample W2).

The REE contents are low and vary from 62–44 ppm in samples J1, W6 and W7, to 23 ppm in sample W2. However, the proportions of specific elements are similar and chondrite-normalized REE patterns for all four samples are parallel, and the patterns themselves are typical of the MORB environment (Fig. 13B). A subtle difference is visible only for positive Eu anomaly in sample W2.

The samples W5a and W5b show very low contents of REE (11 and 13 ppm, respectively), close to the values typical of chondrites. Moreover, these samples reveal identical chondrite-normalized REE patterns and other trace elements patterns (Figs 13C, 13D). The REE diagram demonstrates the presence of positive Eu/Eu* anomaly (1.65 and 1.68, respectively) indicating the cumulate provenance of these rocks.

The sample W3 shows Nb and Ti anomalies (Fig. 13E) as well as moderate enrichment in LREE, but without the Eu anomaly (Fig. 13F). The $(La/Nb)_N$ ratio of 4.27 is the highest value among all studied samples from the Leszczyniec Unit.

The samples W1 and W4 reveal different geochemical signatures. Distinct, negative Nb anomaly occurring in both samples (Fig. 13G) is a feature characteristic for middle/upper crust (Taylor & McLennan, 1985). The chondrite-normalized REE pattern demonstrates distinct, negative Eu anomaly. The LREE plot in both samples is similar to that from sample W5.

The HREE pattern is very similar (almost flat) in all studied samples (Figs 13B, 13D, 13F), except for sample W1, which reveals untypical enrichment in HREE (Fig. 13H).

DISCUSSION

The origin of rocks

Metabasites from the Leszczyniec complex, represented by amphibolites (J1, J2, J3, W6, W7) and chlorite-albite-calcite schists (W5a, W5b), reveal poorly defined foliation and the presence of relic magmatic structures such as the vesicles (J1, J3), well-known from the ocean-floor basalts, and microophitic structures (W5a). The low SiO_2 contents are typical of basalts. Amphibolites J1, W6 and W7 have the REE patterns typical of the MORB environment, whereas the REE patterns of W5a and W5b chlorite-albite-calcite schists indicate cumulate-related origin. Therefore, it is very probable that the protoliths of the studied metabasites from the Leszczyniec complex were lavas generated by the submarine basaltic volcanism. Differences in structures of metabasites presumably reflect the primary diversity of protoliths, as, *e.g*., crystal size, vesicles or fluidal structures. It must be emphasized that metamorphism and weathering (and enrichment in pyrite, as in samples W5a, W5b) affected neither the contents or the proportions of the

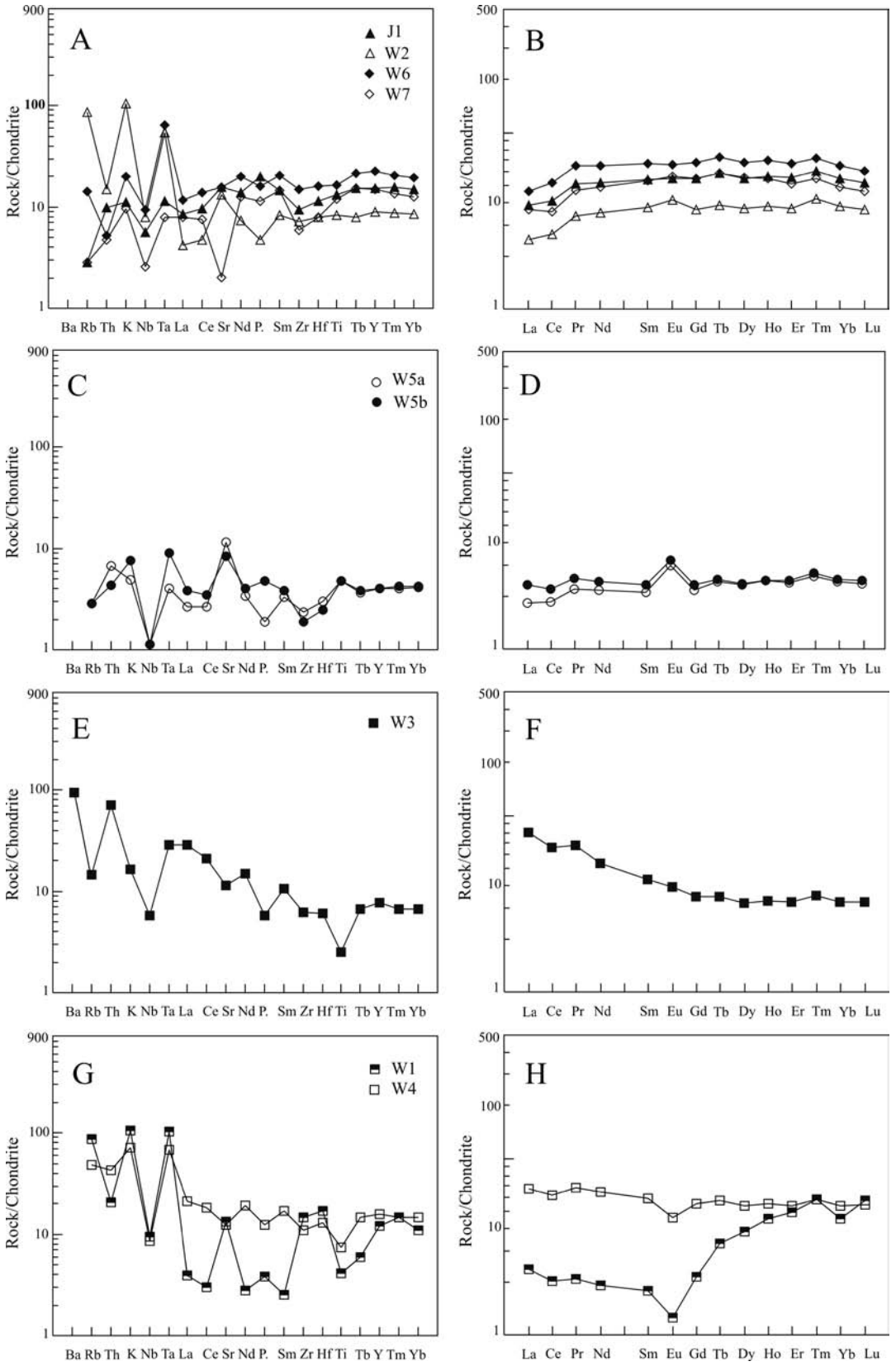

Fig. 13. Chondrite-normalized diagrams for metabasites and pyrite-bearing schists from the Leszczyniec Unit. **A**, **C**, **E**, **G** – multi-element diagrams; normalization values after Thompson (1982): **B**, **D**, **F**, **H** – REE diagrams; normalization values after Nakamura (1974) with additions from Haskin *et al*. (1968). Sampling sites: J1 – Jarkowice, W6, W7 – amphibolite quarry WSW from Wieściszowice village, W1, W2, W3, W4, W5a, W5b – open pit of pyrite-bearing schists in Wieściszowice

REE nor, probably, also the major elements. The most significant differences are seen in the case of incompatible trace elements.

The REE patterns, very similar to those for amphibolites from samples J1, W6 and W7, were found for the chlorite-muscovite-(paragonite)-albite schist (W2), collec- ted in the abandoned Wieściszowice pyrite open pit mine. The schist shows low content of SiO_2, high content of Al_2O_3 and alkalies. Such geochemical signature supported by the presence of chlorite, albite and white, paragonite-muscovite mica seems to confirm our hypothesis that the schist from sample W2 was formed from basaltic tuff, which has been deposited, weathered and altered by hydrothermal fluids in the ocean floor environment (Honnorez, 2003).

The origin of chlorite-albite-quartz-muscovite schist (W3) is unclear. Compared to other rocks from the Leszczyniec Unit, this schist is untypically enriched in LREE, which resembles to some extent the intra-plate basalts. However, the flat HREE sector of the pattern (Fig. 13F) together with the content of REE are similar to those for the MORB (see Fig. 13B). The relatively high content of SiO_2 and low content of Al_2O_3 as well as distinct diversification of the rock into domains enriched and depleted in chlorite and albite suggest the tuffaceous-terrigenous protolith of this rock.

The muscovite-quartz-albite schists (W1) and quartz-albite schists (W4) are presumably the products of metamorphism of acid tuffs with an admixture of terrigenous material. The presence of tuffogenous component is documented by the REE patterns resembling those of felsic rocks from the Leszczyniec Unit (Kryza *et al.*, 1995). The quartz clasts, albite-quartz clasts (sample W1, Fig. 6E) and muscovite clasts (sample W4, Fig. 6A) indicate presence of the terrigenous material.

Summing up, the studied rocks from the Leszczyniec Unit belong to the three genetic groups. The first group includes amphibolites (samples J1, J2, J3, W6, W7) and chlorite-albite-calcite schists (W5), which are metamorphosed products of basic volcanism, mostly ocean-floor lava flows. The second group consists of schists formed during the metamorphism of basic tuffs (sample W2) subjected to pre-metamorphic weathering and hydrothermal alterations. The tuffaceous-terrigenous sediments represented by sample W3 belong to the same group. The protoliths of the third group were acid and intermediate tuffs with an admixture of terrigenous material. The fine-grained size of these rocks suggests deposition in environments distant from the shoreline and/or low rate of erosion at the continent.

The coexistence of the MORB-type lavas with acid tuffs may imply that the rocks of the Leszczyniec Unit formed in the immature oceanic rift environment (Kryza *et al.*, 1995).

The origin of ore mineralization

The rocks interpreted above and the geotectonic environment of their formations were the controls of both types of the ore mineralization encountered in the studied areas:

– the magnetite mineralization in the Area I - Jarkowice; and

– the pyrite ore deposit in the Area II - Wieściszowice.

The magnetite mineralization in the Area I - Jarkowice comprises disseminated grains inherited after the magmatic protolith and microscopic-size aggregates of magnetite rimming the nodules or distributed concordantly to the foliation formed during metamorphism. All macroscopic-size magnetite accumulations are related to the zones of ductile (mylonitization) and brittle (breccias) deformations, younger than the main deformation phase responsible for the origin of foliation and lineation. In these zones, magnetite formed partly at the expense of rock-forming minerals containing Fe and, partly, it resulted from hydrothermal replacement of host rocks by Fe-rich fluids of unknown provenance (Sillitoe & Burrows, 2003) supplied through tectonic zones, which might have played the role of pathways of hydrothermal fluids.

Apart from magnetite textures, also magnetite composition (Ti-poor, near end-member magnetite; Table 1) indicates its metamorphic origin.

The pyrite mineralization in the Area II - Wieściszowice probably formed penecontemporaneously with the protoliths of the schists and protoliths of metaigneous rocks, the age of which was determined with the U-Pb isotopes (zircon method) as 505±5 and 494±2 Ma (Oliver *et al.*, 1993).

Apart from chlorite-albite-calcite schists (W5), the pyrite-bearing schists are metamorphosed tuffs or sedimentary rocks with high admixture of tuffaceous material. Such host-rocks document the genetic link of the Wieściszowice pyrite deposit to the volcanic massive sulphides (VMS) – sedimentary exhalative deposits (SEDEX). This conclusion generally supports the earlier genetic concept presented by Jaskólski (1964) on sedimentary-exhalative genesis of the Wieściszowice ores related to geosynclinal environment, on the contrary to Berg (1913) and Petrascheck (1933) who preferred sedimentary genetic model later transformed by the regional metamorphism.

According to Robb (2004), both the VMS and the SEDEX deposits formed generally during the same geological processes. The ore accumulations in the SEDEX deposits originate from the discharge of hydrothermal fluids at the ocean floor but, on the contrary to the VMS, no clear link to a particular volcanic vent or center can be proved.

The Wieściszowice pyrite deposit meets some of the basic diagnostic features distinguished by Misra (2000) for the distal VMS deposit: (i) coexistence with mixed, volcanic-sedimentary pile, (ii) domination of pyrite but depletion in Cu, (iii) the lack of metal zoning, and (iv) the lack of alteration beneath the ore body.

The differences of the Wieściszowice deposit in relation to the VMS model after Misra (2000) are: (i) the lack of massive sulphide ores, (ii) the lack of stockwork feeder mineralization, and (iii) almost monomineral character of the ore (only trace amounts of chalcopyrite, galena and tennantite were found). However, it can be hypothesized that the present ore mineralization in Wieściszowice is only the preserved fragment of a larger VMS deposit; precisely, it is the disseminated ore formed beneath or at the periphery of the main, massive sulphide ore body, which might have been removed by erosion prior to the regional metamorphism. Obviously, a more precise categorization of the

Wieściszowice deposit within the VMS group brings many difficulties.

The alternative explanation is based on general features of the Leszczyniec complex interpreted as an extensional rift environment (Kryza *et al.* 1995), but not the mature, mid-ocean rift (Mazur & Aleksandrowski, 2001). Hence, the genetic model can be evoked of recent accumulations of metal-bearing sediments forming in the initial rift environment, *e.g.*, the Red Sea (see Deggens & Ross, 1976). Furthermore, if the model of hydrothermal plume presented by Sato (1972, *vide* Mitchell & Garson, 1981) is considered, the features of the ore mineralization discussed above enable us to hypothesize the model of the Wieściszowice deposit as a product of initial rift ore-forming system (*e.g.*, Red-Sea-like). In such an interpretation, hydrothermal fluids were either low-density or were diluted by the sea water and, thus, might have migrated away from the volcanic center. Consequently, such a plume might have produced disseminated mineralization, on the contrary to proximal parts of the Red Sea system, *i.e.* pools filled with concentrated, metalliferous brine, which can illustrate the environment of the massive sulphide ores formation. The distal deposition is a part of the VMS deposits model presented by Franklin (1993).

The influence of metamorphism on ore mineralization

The metamorphic history of rocks from the Leszczyniec Unit includes two or three stages. According to Smulikowski (1999), these are: stage I – ocean-floor metamorphism, stage II – high P/T metamorphism, and stage III – medium- or low-pressure greenschist facies metamorphism. Kryza and Mazur (1995) distinguished two stages: stage I – HP/MT metamorphism and stage II – MP/LT metamorphism. However, these stages are valid mostly for the southern part of the Leszczyniec Unit whereas the history of metamorphism of rocks from the Wieściszowice area has not been studied in detail up to date. Also, the difference in the grade of metamorphism of pyrite-bearing schists and adjacent amphibolites has not been explained in the available literature.

The presence of ocean-floor metamorphism which affected rocks of the Leszczyniec Unit was assumed by Szałamacha and Szałamacha (1991), Smulikowski (1995, 1999), Kryza and Mazur (1995) and Kozdrój (2003). Such metamorphism should have taken place prior to the regional metamorphism and the deformation event, which produced the penetrative foliation and lineation. In the Leszczyniec metabasites, both the foliation and lineation are defined by the bluish-green, low-Ti hornblende, which also forms rims around the older, higher-Ti, olive hornblende (Smulikowski, 1999) or composes marginal zones of amphibole crystals, up to 5 mm in size, imitating the igneous phenocrysts. In such crystals, the core is composed of actinolite (Kryza & Mazur, 1995).

The presence of olive-green hornblende in the cores of some amphibole grains and actinolite in the cores of other amphibole grains indicates that the primary mafic minerals in the Leszczyniec basites were replaced by amphiboles belonging to a different metamorphic facies before the first tectonometamorphic event, when the crystallization of bluish-green hornblende, both surrounding amphibole cores and defining metamorphic foliation, took place.

The local transformations of rocks preceding the regional metamorphism were even more advanced. In pyrite-bearing metabasites from Wieściszowice (sample W5), these transformations led to the complete replacement of mafic minerals by chlorite and plagioclases by albite. Despite such advanced changes of mineral composition, the relics of the microophitic structures are still preserved.

The coexistence of mineral assemblages indicating various conditions of metamorphism demonstrates the lack of equilibrium, which, together with preserved magmatic structures, is typical of the ocean-floor metamorphism resembling the hydrothermal metamorphism (Bucher & Frey, 1994; Honnorez, 2003). However, the Leszczyniec metabasites do not show some features accepted as typical of this metamorphism, such as changes of bulk chemical compositions of rocks or spatial connections between mineral changes of the rocks and fractures used for circulation of sea water through the hot rocks. The lack of these features can be explained by their obliteration during later deformations and does not exclude the hydrothermal alterations. The insignificant effects of these alterations (*e.g.*, the preserved, original magmatic structure) suggest that these processes proceeded at some distance from the active hydrothermal fluid up-flow zones (vents). On the other hand, the lack of changes of the bulk chemical composition of rocks, especially in the case of most of trace elements and the REE, point to the isochemical character of metamorphism, typical of the burial metamorphism. From this point of view, it is possible that the Leszczyniec basites underwent the ocean-floor metamorphism *sensu* Miyashiro (1973) who regarded it as kind of burial metamorphism in high-heat-flow regions of the oceanic ridge crests (Honnorez, 2003).

The action of hydrothermal fluids caused transformations of minerals also in the sediments and tuffs, from which the Wieściszowice schists have originated. The circulation of fluids having temperatures from 250 to 370°C (Honorez, 2003) resulted in crystallization of paragonite and paragonite-chlorite intergrowths. Moreover, these fluids presumably supplied sulphur ions, which reacted with iron present in the sediments. The lack of positive correlation between the contents of Fe_2O_3 and sulphur suggests that only sulphur was supplied to the sediments, presumably from volcanic exhalations.

The weak effects of the ocean-floor metamorphism demonstrate that most of the rocks of the metaigneous Leszczyniec Unit subjected to the action of hydrothermal fluids were rather distant from the active volcanic centres. Only the rocks from Wieściszowice, in which paragonite and pyrite have crystallized, were deposited closer to such centres (see Honorez, 2003), but the monotonous, pyrite-dominated composition of the ore mineralization seems to favour the deposition in the peripheries rather than in the centres of hydrothermal fluids discharge.

The two-stage regional metamorphism and related D_1 and D_2 deformations could not obliterate the earlier changes of mineral composition of metabasites caused by the ocean-floor metamorphism, particularly strong effects of

circulation of hydrothermal fluids within the protoliths of the Wieściszowice pyrite-bearing rocks. The heterogenous strain caused that tectonic structures, foliation, lineation and folds connected with D_1 and D_2 deformation events were concentrated in narrow zones (Mazur & Aleksandrowski, 2001) leaving the rest of the rocks untouched or only slightly deformed. Mineral assemblages related to these structures prove that D_1 deformation proceeded under the conditions of epidote-amphibolite facies (Kryza & Mazur, 1995) whereas the D_2 deformation took place under the greenschist facies conditions.

The regional metamorphism of age estimated as 360–340 Ma (Mazur & Aleksandrowski, 2001) and related deformations have played a significant role in the structure of the ore mineralization recently observed in the rocks of the Leszczyniec Unit. The magnetite mineralization is clearly connected with the zones of ductile and brittle deformations developed during D_2 deformation event.

In the pyrite-bearing schists, the distinguishing of the products of both stages of metamorphism and deformations is more difficult. It seems likely that both stages proceeded under the similar conditions and were continuous. Mineral assemblages formed during hydrothermal replacement generally remained intact although most of minerals recrystallized and was included into the domains defining the foliation and the lineation. However, the comparison of the chemical compositions of inner and outer parts of the rotated paragonite and muscovite porphyroclasts, and their strain fringes enable us to suggest that the composite of white mica have evolved from high-Na to high-K varieties.

The moment in which pyrite crystallized is unclear. The microstructural criteria as, for instance, the participation of pyrite crystals in the formation of first generation of folds, the multistage development of strain fringes and the disruption of grains demonstrate that pyrite was subjected to the both stages of deformation. At the end of the second stage of deformation the fluids were mobilized, which led to crystallization of dolomite and fluorite in sample W4, to corrosion of pyrite crystals and to the filling of cracks in pyrite with chalcopyrite and tennantite. The younger event was the formation of quartz veins, in which small amounts of ore minerals have crystallized.

Age of the ore mineralization

The age of protoliths of metabasites from the Leszczyniec Unit was constrained to 505±5 and 494±2 Ma (U-Pb, zircon method; Oliver *et al.*, 1993). The same age should be accepted for protoliths of pyrite-bearing schists represented by basic tuffs and tuffaceous-terrigenous sediments accompanying basites. The Re-Os isotopic age of pyrite from the Wieściszowice deposit of ~470 Ma is about 25–35 Ma younger than the age of basites, but much older than the age of metamorphism estimated as 360–340 Ma (Mazur & Aleksandrowski, 2001). The age of ~470 Ma indicates that pyrite mineralization was genetically related rather to the ocean-floor environment than to younger hydrothermal processes. It may also indicate that pyrite has retained a part of the age information under metamorphic conditions.

The activity of fluids at the end of the second stage of deformation at ~340 Ma (Mazur & Aleksandrowski, 2001), leading to corrosion of pyrite crystals, might have partially disturbed the Re-Os isotope system in pyrite. These could cause that the Re-Os isotope ages of pyrite are younger than the age of protoliths of rocks from the Leszczyniec Unit.

CONCLUSIONS

1 .The results of our studies confirm the earlier opinions (Kryza *et al.*, 1995; Winchester *et al.*, 1995) that meta-igneous rocks from the Leszczyniec Unit formed in an oceanic rift environment. Igneous rocks were accompanied by tuffs and tuffites.

2. The igneous rocks were subjected to the ocean-floor metamorphism and the accompanying sediments were hydrothermally altered. These processes were followed by the changes resulting from the regional metamorphism.

3. The regional metamorphism did not obliterate the record of earlier geological history rocks of the Leszczyniec Unit.

4. In the Area I - Jarkowice, the “primary” magnetite forms disseminated grains and local, microscopic-scale aggregates in foliated metabasites. Larger concentrations of magnetite are related to the zones of ductile and brittle deformations originating from the D_2 deformation stage. Magnetite was formed at the expense of Fe-bearing rock-forming minerals or Fe ions were supplied from a nearby source.

5. The protoliths of pyrite-bearing schists in the Area II - Wieściszowice were acid and basic tuffs with an admixture of terrigenous material, and ocean-floor basalts. These rocks were hydrothermally altered prior to the regional metamorphism by fluids enriched in sulphur, which promoted crystallization of pyrite. The sources of hydrothermal fluids were the magmatic centres.

6. The genetic model of pyrite mineralization in Wieściszowice deposit might have been the VMS deposition.

7. The age of pyrite crystallization corresponds to the age of rocks of the Leszczyniec Unit.

8. The Re-Os isotope age of pyrite (isochrone ~470 Ma) is about 25–35 Ma younger than the age of protoliths of the Leszczyniec Unit rocks (505–494 Ma; Oliver *et al.*, 1993), possibly due to the activity of fluids circulating during the regional metamorphism.

Acknowledgements

This research was carried out under the Project MNiI 5T12B 036 25 of the Polish Committee for Scientific Research (KBN). Prof. Z. Sawłowicz and Dr. P. Uher are thanked for their constructive reviews. Dr. P. Dzierżanowski and Ms. L. Jeżak are acknowledged for their help and assistance with EMP analyses. Ing. W. Raczek and Dr. S. Madej are thanked for XRF analysis of paragonite.

REFERENCES

Berg, G., 1913. *Die Erzlagerstätten der nördlichen Sudeten.* Festschrift XII, allg. deutsch Bergmannstag Breslau 1913. T. I. Beitrag z. Geol. Ostdtsch., Berlin, 47 pp.

Berg, G., 1938. *Erläuterungen zur Geologische Karte von Preussen und benachbarten deutschen Ländern 1 : 25 000 Blatt Kupferberg*. Preussische Geologische Landesanstalt, Berlin.

Bucher, K. & Frey, M., 1994. *Petrogenesis of metamorphic rocks*. Springer Verlag, Berlin, Heidelberg, New York, 318 pp.

Cathelineau, M., 1988. Cation site occupancy in chlorites and illites as a function of temperature. *Clay Minerals*, 23: 471–485.

Chaloupský, J., Červenka, J., Jetel, J., Králik, F., Libalová, J., Přchová, E., Pokorný, J., Pošmourný, K, Sekyra, J., Shřbený, O., Šalanský, K., Šrámek, J. & Václ, J., 1989. *Geology of the Krkonoše and Jizerské hory Mts*. (In Czech, English summary). Ústředni ústav geologický, Praha, 288 pp.

Deggens, E. T. & Ross, D. A., 1976. Strata-bound metalliferous deposits found in or near active rifts. In: Wolf, J. (*ed.*), *Handbook of strata-bound and stratiform ore deposits, Volume 4, Tectonics and metamorphism*. Elsevier, Amsterdam: 165–202.

Duthou, J. L., Couturie, J. P., Mierzejewski, M. P. & Pin, C., 1991. Next dating of granite sample from the Karkonosze Mountains using Rb-Sr total rock isochrone method. (In Polish, English summary). *Przegląd Geologiczny*, 36: 75–79.

Dziedzic, K. & Teisseyre, A. K., 1990. The Hercynian molasse and younger deposits in the Intra-Sudetic Depression, SW Poland. *Neues Jahrbuch für Geologie and Paläontologie, Abhandlungen*, 179: 285–305.

Fedak, J. & Lindner, M., 1966. Metallogenesis of the Sudetes. *Prace Instytutu Geologicznego*, 5-214: 1–315.

Franklin, J. M., 1993. Volcanic-associated Massive Sulphide Deposits. In: Kirkham, R. V., Sinclair, W. D., Thorpe, R. I. & Duke, J. M. (*eds*), *Mineral Deposit Modelling. Geological Association of Canada Special Paper*, 40: 315–334.

Giorgetti, G., Monecke, T., Kleeberg, R. & Herzig, P. P., 2003. Intermediate sodium-potassium mica in hydrothermally altered rocks of the Waterloo deposit, Australia: a combined SEM-EMP-TEM study. *Contributions to Mineralogy and Petrology*, 146: 159–173.

Guidotti, C. V. & Sassi, F. P., 1998. Petrogenetic significance of Na-K white mica mineralogy: Recent advances for metamorphic rocks. *European Journal of Mineralogy*, 10: 815–854.

Haskin, L. A., Haskin, M. A., Frey, F. A. & Wildeman, T. R., 1968. Relative and absolute terrestrial abundances of the rare earths. In: Ahrens, L. H. (*ed*.), *Origin and distribution of the elements*, 1. Pergamon, Oxford: 889–911.

Honnorez, J., 2003. Hydrothermal alteration vs. ocean-floor metamorphism. A comparison between two case histories: the TAG hydrothermal mound (Mid-Atlantic Ridge) vs. DSDP/ODP Hole 504B (Equatorial East Pacific). *Comptes Rendus Geoscience*, 335: 781–824.

Jaskólski, S., 1964. On the origin of pyrite schists of Wieściszowice (Lower Silesia). (In Polish, English summary). *Rocznik Polskiego Towarzystwa Geolologicznego*, 34: 29–64.

Kozdrój, W., 2003. Geotectonic evolution of the East Karkonosze crystalline complex. (In Polish, English summary). In: Ciężkowski, W., Wojewoda, J. & Żelaźniewicz, A. (*eds*), *Sudety Zachodnie: od wendu do czwartorzędu*. WIND, Wrocław: 67–80.

Krajewski, R., 1949. Report on research concerning pyriteferous shales in Wieściszowice. (In Polish, English summary). *Biuletyn Państwowego Instytutu Geologicznego*, 54: 87–91.

Kretz, R. 1983. Symbols for rock-forming minerals. *American Mineralogist,* 68: 277–79.

Kröner, A., Hegner, E., Hammer, J., Haase, G., Bielicki, K-H., Krauss, M. & Eidam, J., 1994. Geochronology and Nd-Sm systematics of Lusatian granitoids: significance for the evolution of the Variscan orogen in east-central Europe. *Geologische Rundschau*, 83: 357–376.

Kryza, R. & Mazur, S., 1995. Contrasting metamorphic paths in the SE part of the Karkonosze-Izera Block (Western Sudetes, SW Poland). *Neues Jahrbuch für Mineralogie, Abhandlungen*, 169: 157–192.

Kryza, R., Mazur, S. & Pin, C., 1995. Leszczyniec meta-igneous complex in the eastern part of the Karkonosze-Izera Block, Western Sudetes: trace element and Nd isotope study. *Neues Jahrbuch für Mineralogie, Abhandlungen*, 170: 59–74.

Lis, J. & Sylwestrzak, H., 1986. *Minerały Dolnego Śląska*. (In Polish). Wydawnictwa Geologiczne, Warszawa, 791 pp.

Livi, K. J. T., Christidis, G. E., Arkai, P. & Veblen, D. R., 2008. White mica domain formation: A model for paragonite, margarite, and muscovite formation during prograde metamorphism. *American Mineralogist*, 93: 520–527.

Machowiak, K & Armstrong, R., 2007. SHRIMP U-Pb zircon age from the Karkonosze granite. *Mineralogia Polonica (Special Papers)*, 31: 193–196.

Maluski, H. & Patočka, F., 1997. Geochemistry and ^{40}Ar-^{39}Ar geochronology of the mafic metavolcanic rocks from the Rýchory Mountains complex (west Sudetes, Bohemian Massif): paleotectonic significance. *Geological Magazine*, 134 (5): 703–716.

Mazur, S., 1995. Structural and metamorphic evolution of the country rocks at the eastern contact of the Karkonosze granite in the southern Rudawy Janowickie Mts and Lasocki Range. (In Polish, English summary). *Geologia Sudetica*, 29: 31–98.

Mazur, S. & Aleksandrowski, P., 2001. The Tepla(?)/Saxothuringian suture in the Karkonosze-Izera Massif, Western Sudetes, Central European Variscides. *International Journal of Earth Sciences (Geologische Rundschau)*, 90: 341–360.

Misra, K. C., 2000. *Understanding Mineral Deposits*. Kluwer Academic Publishers, London, 845 pp.

Mitchell, A. H. G. & Garson, M. S., 1981. *Mineral Deposits and Global Tectonic Settings*. Academic Press, Cambridge, 457 pp.

Miyashiro, A., 1973. *Metamorphism and Metamorphic Belts*. Halsted Press, J. Wiley & Sons, New York, 492 pp.

Morelli, R., Creaser R. A., Selby, D., Kelley, K., Leach, D. & King, A., 2004. Re-Os sulfide geochronology from the Red Dog sediment-hosted Zn-Pb Ag deposit, Alaska. *Economic Geology*, 99: 1569–1576.

Morelli, R. M., Creaser, R. A., Selby, D, Kontak, D. J. & Horne, R. J., 2005. Rhenium-osmium arsenopyrite geochronology of Meguma Group gold deposits, Meguma Terrane, Nova Scotia, Canada: evidence for multiple gold mineralizing events. *Economic Geology*, 100: 1229–1242.

Nakamura, N., 1974. Determination of REE, Ba, Fe, Mg, Na and K in carbonaceous and ordinary chondrites. *Geochimica et Cosmochimica Acta*, 38: 757–775.

Narębski, W., 1980. Paleotectonic setting of Circum-Karkonosze Lower Paleozoic Spilite-Keratophyre Suites based on geochemistry of iron group elements. *Rocznik Polskiego Towarzystwa Geologicznego*, 50: 3–25.

Nielubowicz, R., 1958. The problem of the pyrite-bearing schists deposit in Wieściszowice. (In Polish). *Przegląd Górniczy*, 10: 541–548.

Oberc, J., 1960. Eastern Karkonosze tectonics and their position in the Sudeten structure. (In Polish, English summary). *Acta Geologica Polonica,* 10: 1–48.

Oberc-Dziedzic, T., 2003. The Izera granites: an attempt of the reconstruction of predeformational history. (In Polish, English summary). In: Ciężkowski, W., Wojewoda, J. & Żelaźnie-

wicz, A. (*eds*), *Sudety Zachodnie: od wendu do czwartorzędu*, WIND, Wrocław: 41–52.

Oberc-Dziedzic, T., Kryza, R., Mochnacka, K. & Larionov, A., 2010. Ordovician passive continental margin magmatism in the Central-European Variscides: U–Pb zircon data from the SE part of the Karkonosze-Izera Massif, Sudetes, SW Poland. *International Journal of Earth Sciences (Geologische Rundschau)*, 99: 27–46.

Oliver, G. J. H., Corfu, F. & Krogh, T. E., 1993. U-Pb ages from SW Poland: evidence for a Caledonian suture zone between Baltica and Gondwana. *Journal of the Geological Society of London*, 150: 355–369.

Parafiniuk, J., 1991. Fibroferrite, slavikite and pickeringite from the oxidation zone of pyrite-bearing schists in Wieściszowice (Lower Silesia). *Mineralogia Polonica*, 22: 3–15.

Parafiniuk, J., 1996. Sulfate minerals and their origin in the weathering zone of the pyrite-bearing schists at Wieściszowice (Rudawy Janowickie Mts, Western Sudetes). *Acta Geologica Polonica*, 46: 353–414.

Parafiniuk, J., Dobrzycki, Ł. & Woźniak, K. 2010. Slavikite-Revision of chemical composition and crystal structure. *American Mineralogist*, 95 (1): 11–18.

Passchier, C. W. & Trouw, R. A. J., 2005. *Microtectonics*. Springer, Berlin, Heidelberg, New York, 366 pp.

Petrascheck, W. E., 1933. Die Erzlagerstätten des Schlesischen Gebirges. *Archiv für Lagerstättenforschung*, H. 59, Berlin: 4–53.

Piestrzyński, A. & Salamon, W., 1977. New data on polymetallic mineralization of quartz veins in the Wieściszowice pyrite deposit. (In Polish, English summary). *Kwartalnik Geologiczny*, 21: 27–35.

Pin, C., Mierzejewski, M. P. & Duthou, J. L., 1987. Isochronous age Rb/Sr of Karkonosze granite from the quarry Szklarska Poręba Huta and significance of initial $^{87}Sr/^{86}Sr$ in this granite. (In Polish, English summary). *Przegląd Geologiczny*, 35: 512–517.

Robb, L., 2004. *Introduction to Ore-Forming Processes*. Blackwell Publishing Co., Oxford, 373 pp.

Roux, J. & Hovis, G. L., 1996. Thermodynamic mixing models for muscovite-paragonite fluids based on solution calorimetric and phase equilibrium data. *Journal of Petrology*, 37: 1241–1254.

Sato, T., 1972. Behaviors of ore-forming fluids in seawater. *Mining Geology*, 22: 31–42.

Schneider, G., 1894. *Die Minerale des Riesen- und Isergebirges*. Wanderer im Riesengebirge, Bd. 6.

Schneiderhöhn, H., 1955. *Erzlagerstätten Kurzvorlesungen zur Einfürung und zur Wiederholung*. Gustav Fischer Verlag, Stuttgart, 375 pp.

Sillitoe, R. H. & Burrows, D. R., 2003 New Field Evidence Bearing on the Origin of the El Laco Magnetite Deposit, Northern Chile – A Reply. *Economic Geology*, 98: 1501–1502.

Smith, R. E., 1967. Segregation vesicles in basaltic lava. *American Journal of Science*, 265: 696–713.

Smulikowski, W., 1995. Evidence for glaucophane-schist facies metamorphism in the East Karkonosze complex, West Sudetes, Poland. *Geologische Rundschau*, 84:720–737.

Smulikowski, W., 1999. Metabasic rocks of the Rudawy Janowickie and Lasocki Range – their significance in the study of metamorphic evolution of the East Karkonosze Complex (West Sudetes, NE Bohemian Massif). *Archiwum Mineralogiczne*, 52: 211–274.

Szałamacha, J., 1969. *Objaśnienia do Szczegółowej mapy geologicznej Sudetów w skali 1:25 000, arkusz Szczepanów*. (In Polish). Wydawnictwa Geologiczne, Warszawa, 77 pp.

Szałamacha, J. & Szałamacha, M., 1991. Leszczyniec ophiolite in the Rudawy Janowickie Mts. (In Polish, English summary). *Biuletyn Państwowego Instytutu Geologicznego*, 367: 61–86.

Szałamacha, J. & Szałamacha, M., 1994. *Objaśnienia do Szczegółowej mapy geologicznej Sudetów w skali 1:25 000, arkusz* Pisarzowice. (In Polish). Wydawnictwa Geologiczne, Warszawa, 77 pp.

Taylor, S. R. & McLennan, S. M., 1985. *The Continental Crust: Its Composition and Evolution: An Examination of the Geochemical Record Preserved in Sedimentary Rocks*. Blackwell Scientific Publications, 312 pp.

Teisseyre, J. H., 1973. Metamorphic rocks of the Rudawy Janowickie and Lasocki Range. (In Polish, English summary). *Geologia Sudetica*, 8: 7–120.

Thompson, R. N., 1982. British Tertiary volcanic province. *Scottish Journal of Geology*: 18, 49–107.

Vernon, R., 2004. *A practical guide to rock microstructure*. Cambridge University Press, Cambridge, 594 pp.

Whitney, D. L. & Evans, B. W., 2010. Abbreviations for names of rock-forming minerals. *American Mineralogist*, 95: 185–187.

Winchester, J. A. & Floyd, P. A., 1977. Geochemical discrimination of different magma series and their differentiation products using immobile elements. *Chemical Geology*, 20: 325–343.

Winchester, J. A., Floyd, P. A., Chocyk, M., Horbowy, K. & Kozdrój, W., 1995. Geochemistry and tectonic environment of Ordovician meta-igneous rocks in the Rudawy Janowickie Complex, SW Poland. *Journal of the Geological Society of London*, 152: 105–115.

Xie, X., Byerly, G. R. & Ferrell Jr., R. E., 1997. IIb trioctahedral chlorite from the Barberton greenstone belt: crystal structure and rock composition constrains with implications to geothermometry. *Contributions to Mineralogy and Petrology*, 126: 275–291.

Zane, A., Sassi, R. & Guidotti, C. V., 1998. New mineral data on metamorphic chlorite as a petrogenetic indicator mineral, with special regard to greenschist-facies rocks. *Canadian Mineralogist,* 36: 713–726.

Zane, A. & Weiss, Z., 1998. A procedure for classifying rock-forming chlorites based on microprobe data. *Rendiconti Fisiche, Accademia Nazionale dei Lincei*, 9, 9: 51–56.